NASA/TM—2000-209798

A Study of Influencing Factors on the Tensile Response of a Titanium Matrix Composite With Weak Interfacial Bonding

Robert K. Goldberg and Steven M. Arnold
Glenn Research Center, Cleveland, Ohio

March 2000

The NASA STI Program Office . . . in Profile

Since its founding, NASA has been dedicated to the advancement of aeronautics and space science. The NASA Scientific and Technical Information (STI) Program Office plays a key part in helping NASA maintain this important role.

The NASA STI Program Office is operated by Langley Research Center, the Lead Center for NASA's scientific and technical information. The NASA STI Program Office provides access to the NASA STI Database, the largest collection of aeronautical and space science STI in the world. The Program Office is also NASA's institutional mechanism for disseminating the results of its research and development activities. These results are published by NASA in the NASA STI Report Series, which includes the following report types:

- TECHNICAL PUBLICATION. Reports of completed research or a major significant phase of research that present the results of NASA programs and include extensive data or theoretical analysis. Includes compilations of significant scientific and technical data and information deemed to be of continuing reference value. NASA's counterpart of peer-reviewed formal professional papers but has less stringent limitations on manuscript length and extent of graphic presentations.

- TECHNICAL MEMORANDUM. Scientific and technical findings that are preliminary or of specialized interest, e.g., quick release reports, working papers, and bibliographies that contain minimal annotation. Does not contain extensive analysis.

- CONTRACTOR REPORT. Scientific and technical findings by NASA-sponsored contractors and grantees.

- CONFERENCE PUBLICATION. Collected papers from scientific and technical conferences, symposia, seminars, or other meetings sponsored or cosponsored by NASA.

- SPECIAL PUBLICATION. Scientific, technical, or historical information from NASA programs, projects, and missions, often concerned with subjects having substantial public interest.

- TECHNICAL TRANSLATION. English-language translations of foreign scientific and technical material pertinent to NASA's mission.

Specialized services that complement the STI Program Office's diverse offerings include creating custom thesauri, building customized data bases, organizing and publishing research results . . . even providing videos.

For more information about the NASA STI Program Office, see the following:

- Access the NASA STI Program Home Page at ***http://www.sti.nasa.gov***

- E-mail your question via the Internet to help@sti.nasa.gov

- Fax your question to the NASA Access Help Desk at (301) 621-0134

- Telephone the NASA Access Help Desk at (301) 621-0390

- Write to:
  NASA Access Help Desk
  NASA Center for AeroSpace Information
  7121 Standard Drive
  Hanover, MD 21076

NASA/TM—2000-209798

A Study of Influencing Factors on the Tensile Response of a Titanium Matrix Composite With Weak Interfacial Bonding

Robert K. Goldberg and Steven M. Arnold
Glenn Research Center, Cleveland, Ohio

National Aeronautics and
Space Administration

Glenn Research Center

March 2000

Acknowledgments

Thanks must be given to Dr. Thomas Wilt of the University of Akron, who implemented the numerous modifications to the MAC code required for carrying out the analyses presented in this report.

Available from

NASA Center for Aerospace Information
7121 Standard Drive
Hanover, MD 21076
Price Code: A03

National Technical Information Service
5285 Port Royal Road
Springfield, VA 22100
Price Code: A03

A STUDY OF INFLUENCING FACTORS ON THE TENSILE RESPONSE OF A TITANIUM MATRIX COMPOSITE WITH WEAK INTERFACIAL BONDING

Robert K. Goldberg and Steven M. Arnold
National Aeronautics and Space Administration
Glenn Research Center
Cleveland, Ohio 44135

SUMMARY

The generalized method of cells micromechanics model is utilized to analyze the tensile stress-strain response of a representative titanium matrix composite with weak interfacial bonding. The fiber/matrix interface is modeled through application of a displacement discontinuity between the fiber and matrix once a critical debonding stress has been exceeded. Unidirectional composites with loading parallel and perpendicular to the fibers are examined, as well as a cross-ply laminate. For each of the laminates studied, analytically obtained results are compared to experimental data. The application of residual stresses through a cool-down process was found to have a significant effect on the tensile response. For the unidirectional laminate with loading applied perpendicular to the fibers, fiber packing and fiber shape were shown to have a significant effect on the predicted tensile response. Furthermore, the interface was characterized through the use of semi-empirical parameters including an interfacial compliance and a "debond stress;" defined as the stress level across the interface which activates fiber/matrix debonding. The results in this paper demonstrate that if architectural factors are correctly accounted for and the interface is appropriately characterized, the macro-level composite behavior can be correctly predicted without modifying any of the fiber or matrix constituent properties.

INTRODUCTION

The usefulness of titanium matrix composites (TMCs) in the aircraft industry has been intensely studied. Consequently, the need for advanced analytical tools that predict the behavior of these materials has also increased. Particularly important is the ability to model the effects of variations in the local microstructure and material composition on the overall, macroscopic response.

Several factors have been found to play a significant role in the inelastic response (e.g., tensile and creep response) of TMCs; i.e., residual stresses, debonding and architectural effects to name a few. For example, Lerch and Saltzman (ref. 1) conducted an extensive series of experimental and analytical studies on the tensile deformation response of a silicon fiber reinforced TMC, that is, SiC/Ti-15-3. Specifically, when the material was loaded transverse to the fiber direction, the stiffness of the stress-strain curve decreased significantly once a certain stress level was reached. The decrease in stiffness was determined to be the result of interfacial debonding. Two factors were found to contribute to the debonding of the composite. First of all, due to a cool-down from the heat treatment temperature, residual stresses were present in the fiber and matrix, which served to hold the constituents in place. These residual stresses needed to be overcome by mechanical loading in order for debonding to take place. However, Lerch and Saltzman found that the stress levels required for debonding were higher than what could be accounted for by residual stresses alone, indicating that there was also chemical bond strength holding the fiber and the matrix together. Therefore, both the residual stresses and chemical bond strength needed to be overcome by mechanical loading in order for debonding to take place. Expanding upon this study, Lerch et al. (ref. 2) conducted detailed finite element analysis of a $[0/90]_s$ SiC/Ti-15-3 TMC system, using gap elements to represent the fiber/matrix interface and including a cool-down in order to apply residual stresses. From the results of these analyses, the authors determined that interfacial debonding played a significant role in the tensile deformation of the composite, and that correctly incorporating the residual stresses was key in correctly predicting the onset of debonding.

Majumdar and Newaz (ref. 3) also carried out an experimental investigation of a model TMC (SiC/Ti-15-3). Their studies found that when the composite was loaded perpendicular to the fiber direction, the tensile stress-strain curve had three distinct regions. First, an initial linear region occurred (denoted as Stage I, see fig. 7 in ref. 3),

during which the macroscopic behavior was elastic and the fiber and matrix remained well bonded. Second, once interfacial debonding occurs, a second linear region, with a lower stiffness than the original linear region (Stage II) was observed. This decrease in stiffness was a result of fiber/matrix debonding; in that, once debonding took place, the stiff fibers had little contribution to the overall stiffness of the material. Finally, the macroscopic tensile response became nonlinear due to significant inelasticity in the matrix. The region was denoted as Stage III. Supplementary analyses also showed that for the composite examined in this work the debonding was primarily due to the overcoming of residual stresses by mechanical loading, with negligible bond strength. Further discussions on the effects of weak interfacial bonding on the transverse (perpendicular to the fiber) stiffness and strength of titanium matrix composites, including the effects of residual stresses can be found in reference 4.

Robertson and Mall (ref. 5) conducted analytical studies using finite elements and a mechanics of materials based micromechanics approach on a TMC composed of SiC fibers in a TIMETAL 21S[1] matrix. In the course of their analyses, the authors computed tensile stress-strain curves for loading perpendicular to the fiber direction and compared the results to experiments. Residual stresses were applied through a cool down process, and a weak fiber/matrix interface was incorporated into their modeling. Upon examination of the results, the authors determined that the fiber/matrix bond was not due to residual stresses alone. Instead, they hypothesized that the fiber/matrix bonds possessed a finite strength, and debonding would not take place until the chemical or mechanical bonds failed due to the applied load.

Arnold et al., (ref. 6) examined in a qualitative sense the effects of fiber architecture and fiber/matrix bonding on the tensile and creep response of a TMC system (SiC/TIMETAL 21S). The analyses were carried out using the Generalized Method of Cells (GMC) micromechanics method (ref. 7) and its framing computer code MAC (Micromechanics Analysis Code) (ref. 8). The analyses were carried out at elevated temperature; consequently the effects of residual stresses were neglected. The weak fiber/matrix interface was modeled as a distinct constituent with an elastic-perfectly viscoplastic constitutive law. The analyses indicated that both fiber architecture (i.e., the placement and spacing of the fibers within the composite) and interfacial bonding had a significant effect on the tensile and creep response of the composite, particularly when loaded perpendicular to the fiber direction.

The current work[2] expands on the previous work of Arnold et al., (ref. 6) in that it examines *quantitatively* the predictive capabilities of MAC (ref. 8) through the inclusion of residual stress effects and the comparison of experimental results. In the previous work isothermal analyses were conducted at one temperature level (650 °C) and residual stresses due to the cool-down history during heat treatment (processing) were not accounted for in the analysis. Here, the effects of residual stresses are shown to be quite significant with respect to capturing the onset of nonlinearity in the stress/strain curve (the “knee” in the curve) as well as the ultimate longitudinal strain to failure of the composite system. Furthermore, unlike the analyses conducted in (ref. 6), in the current work tensile stress/strain response curves for [0], [90] and [0/90] laminates are compared to actual experimental results obtained at both room and elevated temperature. In this manner, a quantitative as well as qualitative measure of the effects of influencing factors (parameters) such as architecture, residual stresses and interfacial behavior on the tensile response can be examined. Additionally, the quantitative comparison of analytical to experimental results will demonstrate that by properly taking into account factors such as architecture, residual stresses and interface specifications, good correlation’s and predictions can be achieved with experimental data without modifying the fiber or matrix constitutive properties.

ANALYSIS METHODOLOGY

GMC

The generalized method of cells (ref. 7), which is an extension of the micromechanics method known in the literature as the method of cells (ref. 10), is the micromechanics analysis method adopted throughout this study. In the original method of cells, a continuously (or discontinuously) reinforced composite is modeled as a doubly (or triply) periodic array of fibers or inclusions embedded in a matrix phase. The periodic character of the assemblage allows one to identify a repeating unit cell that can be used as a building block to construct the entire composite. The properties of the unit cell are thus representative of the properties of the entire assemblage. The unit cell consists of a

[1]TIMETAL 21S is a registered trademark of TIMET, Titanium Metals Corporation, Toronto, OH.

[2]This work was conducted back in 1996-1997 and is being presented at this time in order to provide expanded documentation of (ref. 9), and background/motivation for a future report (ref. 11).

single fiber subcell surrounded by three matrix subcells for continuous composites, and seven matrix subcells for discontinuous composites, hence the name method of cells. The Cartesian geometry of the repeating unit cell allows one to obtain an approximate solution for the stresses and strains in the individual subcells given some macroscopically homogeneous state of stress or strain applied to the composite. The approximate solution to the thus posed boundary value problem is, in turn, used to determine the macroscopic (average) or effective properties of the composite and the effective stress-strain response in the inelastic region.

In the generalized method of cells for continuous (or discontinuous) multiphased composites, the repeating unit cell is subdivided into an arbitrary number of subcells of phases. Specifically, for a two-dimensional analysis the unit cell is broken up into N_β by N_γ subcells, while for a three-dimensional analysis the unit cell is broken up into N_α by N_β by N_γ subcells (fig. 1). Therefore, this generalization extends the modeling capability of the original method of cells to include the following: (1) inelastic thermomechanical response of multiphased composites, (2) modeling of various fiber (phase) architectures including both shape and packing arrangements, (3) modeling of porosities and damage, and (4) the modeling of interfacial regions around inclusions, including interfacial degradation.

The basic homogenization approach taken in the micromechanical analysis consists essentially of four steps. First, the representative volume element, RVE, (or repeating unit cell) of the periodic composite is identified. Second, the macroscopic or average stress and strain state in terms of the individual microscopic (subcell) stress and strain states is defined. Third, the continuity of tractions and displacements are imposed at the boundaries between constituents. For the case of imperfect fiber/matrix bonding, as will be described shortly a displacement discontinuity is applied between fiber and matrix subcells, which is related to the tractions across the interface. The above three steps, in conjunction with microequilibrium, establish the relationship between micro (subcell) total, thermal and inelastic strains and macro (composite) strains via the relevant concentration tensors. In the fourth and final step, the overall macro constitutive equations of the composite are determined. These four steps form the basis of the micro-to-macro mechanics analysis, which describes the behavior of heterogeneous media (refs. 12 and 13). The resulting micromechanical analysis establishes the overall (macro) behavior of the multiphased composite and is expressed as a constitutive relation between the average stress, strain, thermal strain and inelastic strain, in conjunction with the effective elastic stiffness tensor.

The resulting analytic constitutive law has been readily applied to investigate the behavior of various types of composites, given knowledge of the behavior of the individual phases. One advantage to this type of methodology is that any type of simple or combined loading (multiaxial states of stress) can be applied irrespective of whether or not symmetry exists. Similarly, one does not have to resort to different boundary condition application strategies. Another advantage of having available an analytical expression representing the macro elastic-thermoinelastic constitutive law, is that it ensures a reduction in computational costs and memory requirements when implementing this methodology, either in a stand-alone situation or within a finite element code (ref. 14). Evidence of this computational savings (in excess of a thousand times) can be found in references 6 and 15, where a comparison between macroscopic stress-strain curves computed using GMC and FEA is made. There it was shown that for the same global response prediction, GMC was over three orders of magnitude faster in speed than the finite element method, and this was for simpler case of perfect bonding between fiber and matrix. In the case of weak interfacial bonding the difference in computational speed would increase even more with little or no loss in accuracy.

To model imperfect fiber/matrix interfaces in metal matrix composites, two approaches are commonly utilized. One approach, which is used for example in reference 6, is to model the interface as a distinct constituent with its own material model. Another approach is to model the effects of interfacial debonding by applying displacement discontinuities between the fiber and matrix (ref. 16). In the case of finite element analyses, the latter approach is accomplished by applying gap elements between the fiber and matrix (ref. 2); whereas in MAC a modified Achenbach and Zhu (ref. 17) interface model has been developed and implemented and will be described in the next section. Furthermore the GMC formulation also admits a wide variety of physically based deformation and life constitutive models, with an example viscoplastic deformation model being discussed in the subsequent section.

FIBER/MATRIX DEBONDING MODEL

Weak interfacial bonding, due to the multilayer coating applied to the fiber prior to consolidation, is known to be present in TMCs (ref. 4) and significantly affects the transverse stiffness and strength of these composites. The fiber/matrix interface has been modeled in MAC by treating the interface as a distinct constituent (ref. 6). Modeling the interface in this manner allowed a consistent multiaxial representation during both loading and unloading of the

interface and the examination of the influence of initial imperfections and induced interfacial damage. However, for the current work, attempts to employ this method to simulate the interface resulted in exceeding long execution times for the analysis. Furthermore, the properties of this interface were unknown and needed to be arbitrarily assigned.

In an attempt to improve the computational efficiency while still capturing the essence of the interfacial behavior, a new "elastic-perfectly plastic" flexible interface model, in the spirit of Achenbach and Zhu (ref. 17) and Jones and Whittier (ref. 18), was devised to model the interfacial behavior. In this method, a jump in the displacement field is applied between the fiber and matrix subcells when a critical debond stress is exceeded, while continuity of the traction vector is maintained. This critical debond stress activation concept was adopted since in at least some composites (ref. 5) the interface does not debond as soon as the stress across the interface becomes tensile (i.e., the mechanical clamping stress due to residual stresses is exceeded). Instead, due to chemical bond strength or other factors, the interface will only debond when a certain nonzero positive stress ("debond stress") is applied across the interface.

Such a concept is fully substantiated, by examining the elevated temperature tensile response of a TMC (SiC/TIMETAL 21S) loaded perpendicular to the fiber direction (see the curve labeled $\sigma_{DB} = 0$ in fig. 7), where it is obvious that both the initial modulus and the knee in the stress-strain curve are significantly under predicted. These results indicated that debonding did not take place as soon as the stresses became tensile, implying that finite bond strength must have existed between the fiber and matrix for this composite. The interface model is described mathematically as follows:

$$\dot{u}_n^I = \begin{cases} 0 & \text{if } \sigma_n^I < \sigma_{DBn} \\ R_n \cdot \dot{\sigma}_n^I & \text{if } \sigma_n^I \geq \sigma_{DBn} \end{cases}$$

$$\dot{u}_t^I = \begin{cases} 0 & \text{if } \sigma_t^I < \sigma_{DBt} \\ R_t \cdot \dot{\sigma}_t^I & \text{if } \sigma_t^I \geq \sigma_{Dtn} \end{cases} \tag{1}$$

where

u_n	displacement component normal to interface I
u_t	displacement component traverse to interface I
σ_n	stress component normal to interface I
σ_t	shear stress component at interface I
R_n	normal interfacial compliance
R_t	tangential (shear) compliance
σ_{DBn}	normal debond strength
σ_{DBt}	tangential (shear) debond strength
	dotted quantities are time derivatives

Note that the interfacial compliance (R_n) measured the degree of displacement discontinuity in the interface, which simulated the degree of debonding which was present. An R_n of zero implied a perfect bond (no debonding), whereas an R_n of infinity implied a fully debonded interface. R_n was also defined by Aboudi (ref. 10) as the ratio of the interfacial thickness to the "Young's modulus" of the interface. Thus, a R_n of zero implied an infinite interfacial modulus, while a R_n of infinity implied an interfacial modulus of zero. The definition of and behavior of R_t was the same as for R_n with the only difference being in the physical interpretation of R_t as the ratio of the thickness of the interface to its "shear modulus." An important point to note is that in actuality the interface is a small area with undefined properties. Therefore, all of the material constants described here as being associated with the interface were in actuality semi-empirical parameters describing the physical mechanisms of debonding which were taking place. The exact processes used to determine the values of the parameters will be described in a later section of this report. Furthermore, in GMC the displacement continuity conditions could be applied to individual subcell boundaries in specific coordinate directions. As will be discussed in greater detail in reference 11, this feature allowed for the simulation of partial interfacial debonding for a unit cell in which multiple subcells were used to model the fiber.

CONSTITUENT CONSTITUTIVE MODELS

For this study, the material analyzed is a representative titanium matrix composite composed of continuous silicon carbide (SCS-6[3]) fibers embedded in the titanium alloy matrix, TIMETAL 21S. The high-strength, high-stiffness, SCS-6 fibers were assumed in this study to be isotropic and linear elastic. Furthermore, as the variation of elastic properties with temperature was relatively small, the following material properties were utilized throughout, and were assumed to be independent of temperature: Young's modulus, E = 400 GPa, Poisson's ratio, $\nu = 0.32$; and coefficient of thermal expansion, $\alpha = 3.78\times^{-6}\ ^{\circ}C^{-1}$.

TIMETAL 21S is a metastable beta titanium alloy, containing ~21 percent alloying additions that has high strength as well as good creep and oxidation resistance. TIMETAL 21S was developed for use in advanced metal matrix composites and its (isotropic) viscoplastic response has been characterized for the model of Bodner and coworkers (refs. 19 and 20), by Kroupa and Neu (ref. 21) as well as a generalized viscoplasticity with potential structure (GVIPS) model (ref. 22) by Arnold et al., (refs. 23 and 24). The GVIPS model of Arnold et al., (refs. 23 and 24) was selected for use in the current study. In this model, specific forms of both the Gibb's and complementary dissipation potentials were chosen such that a complete (i.e., fully associative) potential based multiaxial, nonisothermal, unified viscoplastic model was obtained. This model possesses a tensorial internal state variable and an evolutionary law that has nonlinear kinematic hardening and both thermal and strain induced recovery mechanisms. A unique aspect of this model is the inclusion of nonlinear hardening through the use of a compliance operator, derived from the Gibb's potential, in the evolution law for the back stress. This nonlinear tensorial operator is significant in that it allows both the flow and evolutionary laws to be fully associative (and therefore easily integrated), it greatly influences the multiaxial response under nonproportional load paths, and in the case of nonisothermal histories, it introduces an instantaneous thermal softening mechanism proportional to the rate of change in temperature. In addition to this nonlinear compliance operator, a new, consistent, potential preserving, internal strain unloading criterion was introduced to prevent abnormalities in the predicted stress-strain curves, during unloading and reversed loading of the external variables. These features make GVIPS accurate in relaxation, as well as able to handle any nonproportional loading that may be present in the composite.

The flow and evolution equations were defined as follows:

$$\dot{\varepsilon}^{i}_{ij} = \begin{cases} 0 & \text{if } \hat{F} < 0 \\ \dfrac{3\left\|\dot{\varepsilon}^{i}_{ij}\right\|\Sigma_{ij}}{2\sqrt{J_2'}} & \text{if } \hat{F} \geq 0 \end{cases}$$

$$\dot{A}_{ij} = \begin{cases} Q_{ijmn}E_{mnkl}b_{kl} & \text{if } a_{ij}\Sigma_{ij} < 0 \\ b_{ij} & \text{if } a_{ij}\Sigma_{ij} \geq 0 \end{cases} \tag{2}$$

$$\dot{a}_{ij} = L_{ijkl}\left(\dot{A}_{kl} - \theta_{kl}\dot{T}\right),$$

where the dot represents time differentiation, A_{ij} is the deviatoric back strain tensor, a_{ij} is the deviatoric back stress tensor, and T is temperature. Additional quantities were defined as follows:

$$\left\|\dot{\varepsilon}^{i}_{ij}\right\| = \sqrt{\frac{2}{3}\dot{\varepsilon}^{i}_{ij}\dot{\varepsilon}^{i}_{ij}} = \frac{\mu_o\hat{F}^n}{\kappa}\left(\text{equivalent inelastic strain rate}\right)$$

$$L_{ijkl} = Q^{-1}_{ijkl} = \frac{\kappa_o^2}{3B_0\left(1+B_1pG^{p-1}\right)}\left(\delta_{ik}\delta_{jl} - \frac{3B_1(p-1)G^{p-2}a_{ij}a_{kl}}{\kappa_o^2\left[1+B_1pG^{p-1}(6p-5)\right]}\right)\left(\text{stiffness operator}\right) \tag{3}$$

$$b_{ij} = \dot{\varepsilon}^{i}_{ij} - \left(\frac{3\beta\kappa\dot{\bar{\varepsilon}}^{vp}H_v[Y]}{2\kappa_o^2\sqrt{G}} + \frac{3R_aB_0G^q}{\kappa_o^2}\right)a_{ij}$$

$$\theta_{ij} = \frac{\partial B_0}{\partial T}\left(1+B_1pG^{p-1}\right)\frac{3a_{ij}}{\kappa_o^2}\left(\text{dynamic thermal recovery operator}\right)$$

[3]SCS-6 is a registered trademark of Textron Systems Division.

where

$$\hat{F} = \left\langle \frac{\sqrt{J_2'}}{\kappa} - Y \right\rangle \text{ (threshold function)}$$

$$Y = \left\langle 1 - \beta\sqrt{\hat{G}} \right\rangle \text{ (yield stress function)} \tag{4}$$

$$\hat{G} = \frac{I_2'}{\kappa_o^2} \text{ (back stress function)}$$

$$I_2' = \frac{3}{2} a_{ij} a_{ij}, \qquad J_2' = \frac{3}{2} \Sigma_{ij} \Sigma_{ij} \text{ (stress invariants)}$$

and E_{ijkl} are elastic stiffness coefficients, $H_v[\bullet]$ is the Heaviside unit step function, and <•> are Macauley brackets. The temperature-independent material parameters are: κ_o, n, B_1, p and q, while the temperature-dependent material parameters are: κ, μ_o, B_0, R_α, and Interpolation functions defined by Arnold et al., (ref. 23) were employed to determine the material parameters for TIMETAL 21S at temperatures other than the reference temperature of 650 °C. A limitation of the material characterization was that above 704 °C, material parameters had to be taken as those at 704 °C. Material parameters at various temperatures are taken from (ref. 23) and presented in table I.

COMPARISON OF ANALYTICAL COMPUTATIONS TO EXPERIMENTAL RESULTS

The computationally efficient and comprehensive micromechanics analysis code, MAC, was utilized to obtain all of the results presented in this study. A full description of the usage and capabilities of MAC can be found in reference 8. Unless otherwise specified, a fiber volume fraction of 0.33, which was determined experimentally to be the nominal fiber volume fraction of the actual composite (ref. 23), and a pseudo-square idealization of the fiber shape[4] was utilized. A micrograph showing a portion of the actual specimen that was tested is shown in figure 2. As can be seen in the figure, while the distance between fiber layers (i.e., in the 2-direction, see fig. 3) is relatively constant, the distance between fiber centers within a layer (i.e., in the 3-direction, see fig. 3) varies significantly. The average ratio of the horizontal (3- axis) and vertical (2-axis) distances between fiber centers (R ratio) over the entire specimen was determined to be 1.11. Although, local fiber architecture can have a significant impact on the transverse material behavior (i.e., when a composite is loaded transverse to the fiber direction) it has little or no effect on the longitudinal response (i.e., when a composite is loaded in the fiber direction). Similarly, when a tensile load is applied perpendicular to the fiber direction, fiber/matrix interfacial debonding becomes significant and must be accounted for, whereas in the case of longitudinal loading (parallel with the fiber direction) fiber/matrix interface assumptions have no impact. The “elastic-perfectly plastic” flexible interface model discussed above was utilized to model the interfacial behavior, and will be discussed below.

The behavior of [0], [90] and [0/90] laminates are examined in this report. Applying a longitudinal load parallel with the fiber axis (along the 1-axis in fig. 3) simulated the [0] laminate, whereas applying the load perpendicular (transverse, i.e., along the 2- or 3-axes) to the fiber direction of a unidirectional laminate simulates a [90] laminate. For the [0] and [90] laminates, the doubly periodic, rectangular fiber array, GMC model was utilized (ref. 8). For the [0/90] laminate, the triple periodic, continuous reinforcement, GMC model was used as illustrated in figure 1.

As discussed earlier, residual stresses due to heat treatment have been found to significantly influence the onset of the nonlinear behavior of metal matrix composites. Consequently, in this study the residual stresses incurred during cool-down from heat-treatment (as all prior residuals due to consolidation are assumed to be annealed out) are considered. To incorporate the residual stresses, a uniform temperature cool-down profile is applied from the heat-treatment temperature to the temperature of interest. The starting temperature and cool-down rates were determined from the actual treatment profile. The results were examined at two temperatures of interest, i.e., 23 °C (room temperature, where residual stresses are significant) and 650 °C (elevated temperature, where residual stresses are negligible). In this way, the effects of residual stresses can be explicitly determined. Subsequent to the application of

[4]Although, the actual shape of the fiber is square, due to the averaging nature of the GMC formulation, the stress concentrations that one might expect at the corners are not present, therefore we use the term pseudo-square to remind the reader.

the cool-down profile, a monotonic strain-controlled, tensile test was simulated up to a strain level of 1.4 percent [0] or 2.0 percent for [90] laminates. The total applied strain rate for the [0] and [0/90] laminates was 1.0×10^{-4}/sec, whereas for the [90] laminate it was 1.667×10^{-4}/sec. These total strain rates correspond to those utilized in the actual experiments (refs. 25 and 26).

LONGITUDINAL TENSILE RESPONSE

The simulated and experimental longitudinal tensile stress-strain results at elevated temperature are shown in figure 4, and results obtained at room temperature are shown in figure 5. In both figures, predictions made with and without the incorporation of residual stresses are compared to experimental results obtained by Castelli (ref. 27). Furthermore, in both figures the yield stress (σ_y), defined as deviation from proportionality, is indicated in order to point out graphically the approximate point at which the curves become nonlinear. At elevated temperature, the inclusion of residual stresses had a negligible effect (as expected) on the computed results, clearly indicating that the residual stress level was low at this elevated temperature, since it is near the heat treatment temperature. At room temperature, on the other hand, the residual stresses had a significant impact on the 'yield stress" or the onset of nonlinearity (the "knee" in the curve) in the predicted stress/strain response. In figure 5, σ_y^R represents qualitatively the yield stress when residual stresses were incorporated into the simulation, and σ_y^{NR} represents qualitatively the yield stress when residual stresses were not incorporated into the simulation. Incorporating the residual stresses into the simulation lowered the yield stress in the room temperature tensile stress-strain curve and provided a more favorable match with the experimental results. These results indicated that at room temperature residual stresses were significant and needed to be incorporated into the simulation in order to make accurate predictions.

For both temperature levels, at higher strain levels the analytical simulations predicted stresses slightly higher than observed in the experiments. While some of this discrepancy could be due to inaccuracies in the matrix constitutive model, it may also be due to fiber breakage occurring at higher strain (stress) levels in the experimental tests, which would lead to a softening of the experimental stress-strain curve. The fact that fiber breakage can take place before total failure of the material occurs is support for example by the work of Neu and Roman (ref. 28) and Brindley and Draper (ref. 29).

In order to examine the issue of fiber breakage in more detail and given the fact that the longitudinal composite ultimate strength is dictated by the ultimate tensile strength of the SCS-6 fiber reinforcement, constituent fiber stress versus the total composite strain are superimposed on the overall stress-strain response of figure 5, (see fig. 6). Again, results are shown for cases with and without the incorporation of residual stresses. As the statistically significant ultimate tensile strength of the SCS-6 fiber reinforcement (ref. 30) varies between 2400 and 5170 MPa with the average being ~4140 MPa, we have indicated in figure 6 potential fiber breakage levels (i.e., points A, B and C) starting at 3450 MPa and increasing at 350 MPa increments. Clearly the overall strain level at which these fiber stress levels occur is relatively close to the strain level at which the overall composite fails, with 3622 MPa being an accurate calibration estimate of the effective fiber strength, for both room and elevated temperature (not shown) calculations. Also an important observation relative to the inclusion of residual stresses due to processing can be gleaned from figure 6 in that when residual stresses are not applied, the composite strain level at which potential fiber breakage can occur (i.e., A', B' and C') is significantly lower than the corresponding case with residual stresses. These results indicate that if residual stresses are not applied, the failure stress and strain of the overall composite could be significantly under predicted in an analysis. Consequently, given that the ultimate failure of the composite for this laminate and loading configuration is most likely due to fiber failure, the above results suggest that if an appropriate fiber breakage model was developed for MAC (see ref. 11) the analysis should accurately predict the ultimate longitudinal tensile failure strain of the composite. Additionally, since the actual fiber tensile strength possesses a statistical distribution, see the vendor's histogram (ref. 30), with its average at 4140 MPa, one would expect that if a statistical failure distribution was added to the fiber breakage model in such a way as to capture the stress redistribution occurring due to the accumulation of fiber breaks a softer response (better representing the actual experimental results) would be predicted at high stress (strain) levels. Support for this idea can be seen in figure 6 wherein fiber breakage could initiate at composite stress levels as low as 2400 MPa at room temperature. The 2400 MPa fiber stress level corresponds to a composite strain level of 0.8 percent at which the experimental results become more nonlinear and start to deviate significantly from the computed results. This trend was observed both at room and elevated temperature. The results for both the overall composite and the fiber confirm that proper application of residual stresses can have a significant effect on accurately predicting both the material's deformation behavior and ultimate tensile strength.

TRANSVERSE TENSILE RESPONSE

The transverse (loading perpendicular to the fiber direction) tensile response for the [90] laminate was also simulated using MAC. To apply the transverse loads, strain controlled loading was applied along the 3-direction axis to a level of 2.0 percent at a strain rate of 1.667×10^{-4}/sec. The strain rate was chosen in order to facilitate comparisons to available experimental data found in reference 26. The use of experimental data to correlate and validate the analytical response is the major difference between the current work and the previous work of Arnold et al., (ref. 6). In reference 6, the effects of architecture and the fiber/matrix interface bond were examined strictly from a qualitative viewpoint. Alternatively, in this work, the effects of the various parameters effecting transverse behavior (bond strength and architecture) are examined quantitatively through comparisons with experimental results.

Correlation of Interfacial Parameters

As discussed earlier, TMCs have been found to have a weak fiber/matrix interface and the effects of the interface become significant when tensile loads are applied perpendicular to the fiber direction. For the elastic-perfectly plastic interface model utilized, the debond strength, σ_{DB}, and the interfacial "compliance" need to be determined empirically. For this study, the composite was assumed to be perfectly bonded in the shear direction. Therefore, the tangential "compliance" R_t was set to zero, and the tangential debond strength σ_{DBt} was set to a very high value.

The first parameter to be correlated was the normal debond stress, σ_{DBn}. For these analyses, the normal "compliance" R_n was set to a relatively high value to simulate a fully debonded interface. Simulation results were examined at both elevated temperature (650 °C) (fig. 7) and room temperature (fig. 8) (23 °C) and compared to experimental values (ref. 26). However, the elevated temperature results were the ones used for correlation[5] whereas, the room temperature results were used for verification. For both temperatures, the debond stress was varied from 0 MPa (simulating zero bond strength) to 96.53 MPa. The results at elevated temperature (fig. 7) showed that when the debond stress was set to zero, the initial deviation from linearity (indicating the beginning of debonding) occurred almost immediately after application of the transverse tensile load, and at a much lower stress level than indicated by the experimental results. This was expected since minimal residual stresses were present at this temperature so that with zero bond strength, debonding would occur as soon as residual stresses were overcome. These results clearly indicate, consistent with reference 5, that finite bond strength exists for the SCS-6/TIMETAL 21S composite independent from residual stresses. As the bond strength was increased, the stress level at which deviation from linearity began (again indicating the onset of debonding) increased. A debond stress of 96.53 MPa provided the best correlation between the predicted and experimentally observed deviation from linearity. An interesting point to note is that varying the debond stress only appears to affect the stress level at which debonding commences while the remainder of the stress-strain response curves remain roughly parallel (similar). Considering the room temperature results, shown in figure 8, the initial deviation from linearity is clearly seen to be predicted reasonably well when the value of the debond stress is 96.53 MPa. Alternatively, when the debond stress was set to zero, the stress level at which debonding occurred (indicated by the onset of nonlinearity) was significantly under predicted. However, in sharp contrast to the elevated temperature response (fig. 7) debonding did not occur immediately upon application of the tensile load, due to the higher level of compressive, thermally induced residual stress present at room temperature. These results appeared to confirm that for the SCS-6/TIMETAL 21S composite, both residual stresses and the finite bond strength needed to be overcome in order for debonding to occur at room temperature.

Once the debond stress was correlated, the value of the normal interfacial compliance, R_n was determined. Analytical results were computed for both room and elevated temperature with the value of the interfacial compliance varying from 0 MPa^{-1} (simulating a perfect bond) to a value of 4×10^{-4} MPa^{-1}. Increasing the value of R_n higher than 4×10^{-4} MPa^{-1} did not change the results, which indicated that an R_n value of 4×10^{-4} MPa^{-1} simulated a fully debonded interface. The simulated and experimental (ref. 26) results are shown in figure 9 (elevated temperature) and figure 10 (room temperature). The results in both figures clearly demonstrate that when a perfect bond is assumed (R_n equal to zero) the correlation between the experimental and analytical results is significantly over predicted. Alternatively, simulating a fully debonded interface provided the best correlation to the experimental results,

[5]From longitudinal results, the residual stresses at elevated temeprature were determined to be negligible, consequently the initial deviation from linearity in the macro stress-strain can be attributed solely to the breaking of the fiber/matrix interfacial bond, as no mechancial clamping force (residual stress) is present.

confirming that this material had a weak interface. Note that varying the value of R_n did not affect the stress level at which nonlinearity began, but instead only affected the stiffness and hardening slope of the tensile curve after debonding occurred.

Effects of Residual Stresses

The transverse tensile results presented to this point have included the effects of residual stresses. To further examine the effects of residual stresses on the transverse tensile results, analyses were conducted in which residual stresses were not applied. A four cell rectangular unit cell model with an R-ratio of 1.11 was used for the analyses, with the debond stress and interfacial compliance set to the values determined above. Simulated and experimental (ref. 26) stress-strain curves computed at a temperature of 650 °C (elevated temperature) are shown in figure 11, and results computed at 23 °C (room temperature) are shown in figure 12. As can be seen in the figures, at elevated temperature the application of residual stresses had minimal effect (as expected) on the computed results (particularly for strains less than 0.1 percent), which are consistent with the results obtained for longitudinal tensile loading. Alternatively, at room temperature, when residual stresses were not included the stress level at which debonding occurred was significantly under predicted as compared to the experimental results. Also, the predicted stress values at high macroscopic strain levels are still somewhat higher than the experimental stress values, although the discrepancy is less than was seen at elevated temperature. This trend is consistent with the fact that (1) matrix inelasticity is less significant at room temperature as compared with elevated temperatures and (2) the interfacial model utilized does not allow for proper load shedding from the fiber to the matrix once debonding occurs. This fact will be discussed more fully in the following discussion section. Clearly, these results verify once again that residual stresses need to be incorporated into all lower temperature composite simulations in order to obtain accurate results.

Effects of Fiber Architecture

Once the interface model was correlated, the influence of fiber packing on the transverse tensile response (due to loading along the 3-axis of fig. 3) of the SCS-6/TIMETAL 21S composite was examined for both elevated and room temperature. In these analyses, the normal debond stress and interfacial compliance were assumed to be independent of fiber packing, and the correlated values determined in the previous section were used. Five packing arrangements, which are displayed graphically in figure 13, are examined: square, square diagonal and three rectangular fiber packing (i.e., $R = 0.74$, $R = 1.11$ (which is the average R ratio determined from micrographs for the actual material in (ref. 25) and not shown in fig. 13), and $R = 1.34$). The R-ratio was defined as the ratio of the average distance between fiber centers in the 3-direction (fig. 3) to the average distance between fiber centers in the 2-direction. The square packing arrangement was equivalent to a rectangular pack with an R-ratio of 1.0. These fiber-packing architectures were chosen in order to be consistent with the qualitative analyses conducted in reference 6.

Computed transverse tensile stress strain curves including residual stresses obtained at elevated temperature (650 °C) are shown in figure 14, and results computed at room temperature (23 °C) are shown in figure 15. In both cases, the computed results were compared to experimental results obtained from reference 26. At elevated temperature, the fiber architecture did not appear to have a significant effect on the macroscopic stress level at which debonding occurred (indicated by the onset of nonlinearity). However, the slope of the hardening curve was significantly affected by the fiber packing, with higher R-ratios yielding a softer response. The square diagonal pack resulted in the softest response, which was consistent with the qualitative results obtained by Arnold et al., (ref. 6). However, the very compliant post-yield slope is most likely an artifact of the unit cell model, since the square diagonal unit cell has two fibers which can debond, thus leaving an intact cross-sectional area much smaller than the rectangular unit cell model composed of a single fiber. Consequently, the remaining matrix will carry a greater stress and thus experience an increase in inelastic flow, thus producing a “softer” overall response history. To allow each unit cell model to have equivalent cross-sectional areas, a progressive debonding technique is required. While this capability was not present in MAC at the time these analyses were conducted, the concept has since been incorporated into MAC/GMC and will be discussed in a future report.

The results obtained at room temperature (see fig. 15) indicate once again that increasing the R-ratio results in a softening of the tensile stress-strain curve. Furthermore, once again the square diagonal pack yielded the softest

response. However, in contrast to the elevated temperature results, varying the fiber packing architecture at room temperature also affected the macroscopic stress level at which debonding occurred. These results illustrate that architecture influences residual stress build-up, so that as the R-ratio is increased, the stress at which debonding occurs is decreased. When the results at both temperature levels are examined simultaneously, the analytical results obtained by using a rectangular pack with an R ratio of 1.11 appears to provide a very good match to the experimental values, which is reasonable since the average R ratio measured from micrographs is equal to 1.11. Overall, the results demonstrate that fiber packing has a significant effect on the overall response (and initial residual stress state), and the packing must be correctly modeled in order to correctly predict the material behavior.

Arnold et al. (ref. 6) showed in a qualitative sense that using a more refined unit cell, which more completely approximated a circular fiber, yielded different results in simulations of transverse tensile tests than results computed using a square fiber approximation. Numerous other researchers have also examined the effects of fiber shape on the tensile response of composites, as reviewed and discussed in reference 6. For this study, the effects of varying the fiber shape, while maintaining the same fiber volume fraction and fiber packing were examined quantitatively through comparisons to experimental results. An R-ratio of 1.11 was used, and the interfacial compliance and debond stress values determined earlier were once again employed. A schematic of the unit cell model for the circular fiber is shown in figure 16. An important point to note is that for the refined unit cell model, up to ten subcell interfaces may now debond once the debond stress reached. Loading was again applied along the 3-direction axis as defined in figure 3, and residual stresses were incorporated.

Tensile curves obtained at 650° and 23 °C for both square and circular fiber shapes are shown in figures 17 and 18, along with experimental results (ref. 26), respectively. The elevated temperature results indicated that varying the fiber shape primarily affected the slope of the hardening curve after debonding took place. However, the comparison between the experimental and computed results was much better for the circular fiber model. This result was reasonable since the circular fiber model was more refined than the original square fiber model. The results computed using the circular fiber model at room temperature provided a better comparison to the experimental values in several respects. First of all, the original elastic modulus was predicted more accurately. Secondly, the slight break in the experimental curve at a stress level of ~100 MPa was captured by the circular fiber model. The slight break in the experimental curve indicated that some debonding might have taken place at this point. Since the circular fiber unit cell allowed for the possibility of a gradual debonding, the model could capture this behavior. Furthermore, using the circular fiber model, which provided a better comparison to the experimental results, reduced the stiffness of the hardening curve. Overall, the results indicated that for modeling the transverse tensile response of a composite with a weak fiber/matrix interface, correctly modeling the fiber shape was very important. For the current study, however, one disadvantage of using the circular fiber shape was that the execution time for analyses using circular fibers increased by 20 to 30 times when compared to analyses conducted using square fibers. However, as discussed in reference 11, since the time that the analyses included in this report were conducted, significant modifications have been made to the MAC code which permits more computationally efficient analyses of complex fiber architectures.

Discussion of Transverse Tensile Results

For all of the computed transverse tensile results which have been presented, the three distinct regions of the stress-strain curve described by Majumdar and Newaz (ref. 3) were observed and predicted. Recall that these regions were denoted as follows. First, an initial linear region was present, wherein the macroscopic behavior remained elastic and the fiber and matrix remained bonded. A second linear region occurred next, wherein interfacial debonding occurred and the interface opened. Finally, a third nonlinear region occurred, in which significant matrix inelasticity was present. Furthermore, once the interfacial parameters were appropriately correlated and residual stresses properly accounted for, the computed results compared reasonably well to the experimental values (ref. 26), particularly when a more refined unit cell model was utilized. However, the predictions made at elevated temperature generally over predicted the stresses in the inelastic portion of the tensile response, for reasons to be discussed below.

To further analyze the reasons behind the over prediction of the transverse tensile stresses at elevated temperature, the stress-strain response for each of the individual subcells was examined. In figures 19 and 20 the local stresses in the individual subcells (see fig. 3 for subcell numbering) are plotted; wherein subcell 1 corresponds to the fiber material and subcells 2, 3 and 4 are associated with the matrix material. In figure 19 the microstress verses strain response are shown with the residual strains present at the start of the mechanical loading (i.e., the curves do

not start at a strain value of zero, but at the actual residual strain value present after the cool-down process); whereas, in figure 20, the stress verses the total macroscopic strain in the composite is illustrated. In figure 20, for comparison the predicted total macroscopic transverse tensile stresses are also included in the plot. Furthermore, an analysis was conducted using MAC to simulate the tensile response of the bulk matrix. This analysis was conducted by assuming a negligibly small fiber volume fraction. The results from this additional analysis are also included in the figure (labeled as TIMETAL 21S). Clearly, all four subcells start off with a linear elastic response. Then at a microstress level of 96.5 MPa (the defined "debond stress"), the interface debonds, and the fiber subcell (subcell 1) and the adjoining matrix subcell (subcell 2) remain at a constant stress level. This constant stress is due to the nature of the interfacial debonding model utilized and the traction continuity that is imposed between subcells. The stress level in the two remaining matrix subcells (subcells 3 and 4) continue to increase, and in fact rise sufficiently to induce inelastic behavior in these subcells—thus explaining the onset of the third nonlinear region of the stress-strain curve as discussed above. However, realistically, one would expect the stress in the fiber and the adjoining matrix to reduce to zero subsequent to debonding; with the corresponding debond stress being transferred to the remaining matrix subcells after some time. This additional stress, that is transferred to the other matrix subcells, would most likely promote greater matrix inelasticity and consequently result in a further softening of the predicted macroscopic stress-strain curve; particularly at high temperatures where matrix inelasticity is quite significant. This deficiency in the interfacial model implemented within MAC is thought to be the cause of the over prediction of the macroscopic stress state in the composite. Note, one might question how is it that subcells 3 and 4 (which in this case are associated with the matrix material) can carry a microstress state higher than that of the matrix material itself as shown in figure 20. This is due to the fact that the subcell responses 3 and 4 depicted, are only one component of the multiaxial stress tensor. Consequently, if the effective (J_2) stress response of the matrix verses the macro strain response was plotted (not shown in the fig. 20) both should follow that of the matrix only response quite nicely.

To further illustrate the multiaxial nature of the predicted stress-strain response of the [90] laminate at 650 ^{o}C, the variation of the macroscopic stress in the loading direction is plotted as a function of the macroscopic strain in each of the three coordinate directions in figure 21; that is, 1-1 (parallel to the fiber), 2-2 (perpendicular to the fiber and the loading direction), and 3-3 (perpendicular to the fiber and in the loading direction). Note that once again the symbol σ_y is used to indicate graphically the approximate point at which the response deviates from proportionality. Clearly, the 1-1 response is essentially linear with only very small (Poisson's ratio induced) strain levels being obtained. This response is reasonable and expected, as the response in this direction is dominated by the fiber, which is elastic and has a much higher stiffness than the matrix. Alternatively, in the transverse directions the responses shown indicate a linear region up to the on-set of debonding (Stage I), followed by another linear region at a reduced stiffness (Stage II), followed by significant inelasticity at high macroscopic stress levels (Stage III).

A similar examination to that done above for the elevated temperature tensile test can be conducted for that of the response at room temperature. Again the micro stress-strain response (in the 33-loading, direction) of the individual subcells are plotted in figure 22 whereas, in figure 23 the corresponding subcell and composite stress states are shown versus the macro strain in the 33 direction. Once again, predicted results for the macroscopic composite and the TIMETAL 21S matrix are included for comparison. Similar to our previous elevated temperature observations, once the interface debonds the fiber subcell (subcell 1) and its adjoining matrix subcell (subcell 2) remain at a constant stress level (the "debond stress"), since the present interfacial debond model incorporated does not allow for any load shedding to the remaining matrix subcells. Here, however, the influence (development of residual stress and strain) of the initial cool-down is quite significant and apparent, in that (see figs. 22 and 23) there are significant residual strains in all four subcells (with the fiber subcell having the least amount of residual strain). Note the significant compressive residual stresses present within the fiber subcell and its adjoining matrix subcell (which explains the delay in interfacial debonding), and, the significant tensile residual stresses in the remaining two matrix subcells. Again, examining the variation of the macroscopic stress in the loading direction as a function of the macroscopic strain in each of the three coordinate directions, see figure 24, we see similar behavior to that observed at 650 °C but now the three stages of deformation are more distinct due to the presence of residual stresses.

CROSS-PLY LAMINATE TENSILE RESPONSE

To further validate the developed methodology, the tensile response of a [0/90] cross-ply laminate was simulated. A schematic of the unit cell employed is shown in figure 25. The fiber volume fraction, interfacial parameters and fiber architecture were the same as applied previously for the analyses with transverse tensile loading. Analyses

were again conducted at both 650 °C (elevated temperature) and 23 °C (room temperature). Residual stresses were applied through a cool-down process, and strain controlled tensile loads were subsequently applied along the 3-direction axis (see fig. 25) at a strain rate of 1.0×10^{-4}/sec, in order to match experimental results obtained by Castelli (ref. 31).

Simulated and experimental results (ref. 31) obtained at elevated temperature are shown in figure 26, and results obtained at room temperature are shown in figure 27. To demonstrate the effects of residual stresses, computed results in which residual stresses were not included are also shown in the figures. As shown previously, the incorporation of residual stresses had minimal effects at elevated temperature on the resulting stress-strain response. At room temperature, however, the onset of nonlinearity was significantly effected by residual stresses. When residual stress effects were ignored, the onset of nonlinearity occurred at a much higher strain level (resulting in an over prediction of the stresses) as compared to the experimental results. When residual stresses were incorporated into the analysis, a much better match with the experimental results was obtained. At elevated temperature, there was some discrepancy between the experimental and computed results, which could have been due to the interfacial model formulation, which did not permit load shedding once debonding occurred as discussed earlier in this report. Furthermore, fiber damage prior to final failure might have occurred in the [0°] plies in the experimental tests which was not accounted for in the model (as discussed earlier).

CONCULSIONS

The effects of residual stresses, fiber packing and shape, and the influence of interfacial bonding on the tensile stress strain response of a titanium matrix composite (SCS-6/TIMETAL 21S) has been modeled for a composite under uniaxial longitudinal and transverse loads, as well as for a cross-ply laminate. Additionally, the analytical results have been compared to experimentally obtained results in order to provide a quantitative characterization of the various parameters examined. For all of the laminates studied, proper application of residual stresses was required in order to accurately model the composite response. Furthermore, the fiber architecture needed to be properly described and the fiber/matrix interface needed to be appropriately characterized in order for the analytical response to compare favorably to the experimental results. Through proper characterization of the fiber/matrix interface model described in this work, the stress level at which debonding occurred and the slope of the hardening curve were appropriately simulated. These analyses thus indicated that the generalized method of cells micromechanics model in combination with the generalized viscoplastic potential structure inelastic constitutive model could adequately predict the actual behavior of the material.

Future work will encompass several points. First, as discussed earlier, the interfacial model utilized in this report, while easy to utilize and computationally efficient, has significant deficiencies, particularly in terms of properly shedding load from the fiber to the matrix once debonding has occurred. A need is present to develop an interface model where the interface is modeled as a distinct constituent, with material properties that are different in tension and compression (to account for application of residual stresses), and allows for the proper stress transfer between the fiber and surrounding matrix. Additionally, creep and relaxation analyses, as well as cyclic analyses, should be conducted in order to examine the effects of the parameters studied in this report for loadings other than monotonic tensile loadings.

REFERENCES

1. Lerch, B.A.; and Saltsman, J.F.: Tensile Deformation of SiC/Ti-15-3 Laminates. Composite Materials: Fatigue and Fracture, Fourth Volume, ASTM STP 1156, W.W. Stinchcomb and N.E. Ashbaugh, Eds., American Society for Testing and Materials, pp. 161–175, 1993.
2. Lerch, B.A.; Melis, M.E.; and Tong, M.: Experimental and Analytical Analysis of Stress-Strain Behavior in a $[90^o/0^o]_{2s}$, SiC/Ti-15-3 Laminate. NASA TM–104470, 1991.
3. Majumdar, B.S.; and Newaz, G.M.: Inelastic Deformation of Metal Matrix Composites: Plasticity and Damage Mechanisms. Phil. Mag., Vol. 66, no. 2, pp. 187, 1992.
4. Mall, S.; and Nicholas, T.: Titanium Matrix Composites, Mechanical Behavior. Technomic Publishing Company, Lancaster, PA, 1998.

5. Robertson, D.D.; and Mall, S.: Micromechanical Analysis for Thermoviscoplastic Behavior of Unidirectional Fiber Composites. Comp. Sci. and Tech., Vol. 52, pp. 483, 1994.
6. Arnold, S.M.; Pindera, M.-J.; and Wilt, T.E.: Influence of Fiber Architecture on the Inelastic Response of Metal Matrix Composites. Int. J. of Plasticity, Vol. 12, no. 4, pp. 507, 1996.
7. Paley, M.; and Aboudi, J.: Micromechanical Analysis of Composites by the Generalized Method of Cells Model. Mechanics of Materials, Vol. 14, pp. 127, 1992.
8. Wilt, T.E.; and Arnold, S.M.: Micromechanics Analysis Code (MAC), User Guide: Version 2.0. NASA TM–107290, 1996.
9. Wilt, T.E., Arnold, S.M. and Goldberg, R.: Micromechanics Analysis Code, MAC Features and Applications, HITEMP Review 1997, CP–10192, paper 30, 1997
10. Aboudi, J.: Mechanics of Composite Materials, A Unified Approach. Elsevier, 1991.
11. Bednarcyk, B.A.: To be published
12. Aboudi, J.: Micromechanical Analysis of Composites by the Method of Cells. Applied Mechanics Reviews, Vol. 42, pp. 193, 1993.
13. Aboudi, J.: Micromechanical Analysis of Thermo-Inelastic Multiphase Short-Fiber Composites. NASA CR–195290, 1994.
14. Arnold, S.M, Bednarcyk, B.A., Wilt, T.E., and Trowbridge, D.: Micromechanics Analysis Code With Generalized Method of Cells (MAC/GMC), User Guide: Version 3.0. NASA TM–1999-209070, 1999.
15. Wilt, T.E.: On the Finite Element Implementation of the Generalized Method of Cells Micromechanics Constitutive Model. NASA CR–195451, 1995.
16. Aboudi, J.: Constitutive Equations for Elastoplastic Composites with Imperfect Bonding. Int. J. Plasticity, Vol. 4, pp. 103–125, 1988
17. Achenbach, J.D.; and Zhu, H.: J. Mech. Phys. Solids, Vol. 37, pp. 381, 1989
18. Jones, J.P.; and Whittier, J.S.: J. Appl. Mech. Vol. 34, pp. 905, 1967.
19. Chan, K.S.; Bodner, S.R.; and Lindholm, U.S.: Phenomlogical Modeling of Hardening and Thermal Recovery in Metals, J. Eng. Mater. Technol., Vol. 110, pp. 1, 1988.
20. Chan, K.S.; and Lindholm, U.S.: Inelastic Deformation Under Nonisothermal Loading, J. Eng. Mater. Technol., Vol. 112, pp. 15, 1990.
21. Kroupa, J.L.; and Neu, R.W.: Implementation of a Nonisothermal Unified Inelastic-Strain Theory into ADINA 6.0 for a Titanium Alloy-User Guide. Wright Laboratory WL-TR-93-4005, University of Dayton, Dayton, 1993.
22. Arnold, S.M.; and Saleeb, A.F.: On the Thermodynamic Framework of Generalized Coupled Thermoelastic-Viscoplastic-Damage Modeling. Int. J. Plasticity, Vol. 10, pp. 263, 1994.
23. Arnold, S.M.; Saleeb, A.F.; and Castelli, M.G.: A Fully Associative, Nonisothermal, Nonlinear Kinematic, Unified Viscoplastic Model for Titanium Alloys. Thermo-Mechanical Fatigue Behavior of Materials: Second Volume, ASTM STP–1263, M.J. Verilli and M.G. Castelli, Eds., American Society for Testing and Materials, Philadelphia, pp. 146, 1996.
24. Arnold, S.M.; Saleeb, A.F.; and Castelli, M.G.: A Fully Associative, Nonlinear Kinematic, Unified Viscoplastic Model for Titanium Alloys. Life Prediction Methodology for Titanium Matrix Composites, ASTM STP–1253, W.S. Johnson, J.M. Larsen and B.N. Cox, Eds., Philadelphia, American Society for Testing and Materials, 1996.
25. Castelli, M.G.: Characterization of Damage Progression in SCS-6/TIMETAL 21S $[0]_4$ Under Thermomechanical Fatigue Loadings. NASA CR–195399, 1994.
26. Cervay, R.R.: SCS-6/β21s and SCS-9/β21S Mechanical Property Evaluation. NASP CR–1165, 1994.
27. Castelli, M.G.: Personal Communication, 1995.
28. Neu, R.W.: and Roman, I.: Acoustic Emission Monitoring of Damage in Metal Matrix Composites Subjected to Thermomechanical Fatigue. Comp. Sci. and Tech., Vol. 52, No. 1, pp. 1, 1994.
29. Brindley, P.K. and Draper, S.L.: Failure Mechanisms of 0^o and 90^o SiC/Ti-24Al-11Nb Composites Under Various Loading Conditions. Structural Intermetalics. R. Darolia et al. Eds., The Minerals, Metals and Materials Society, pp. 727–737.
30. Textron Systems Division, Manufacturers Data, Vendor data sheet.
31. Castelli, M.G.: Thermomechanical Fatigue Damage/Failure Mechanisms in SCS-6/TIMETAL 21S $[0/90]_s$ Composite. Composites Engineering, Vol. 4, no. 9, pp. 931, 1994.

TABLE 1.—TI-21S MATERIAL PARAMETERS

	23 °C	300 °C	500 °C	650 °C	704 °C
E (GPa)	114.1	107.9	95.1	80.7	59.7
CTE (μ °C^{-1})	7.717	9.209	10.70	12.13	14.09
κ (MPa)	1029	768.4	254.2	5.861	0.756
μ (MPa/sec)	667.6	137.8	1.45×10^{-3}	6.19×10^{-9}	1.13×10^{-11}
B_0 (MPa)	6.908×10^{-5}	1.035×10^{-4}	2.756×10^{-4}	5.870×10^{-4}	6.346×10^{-4}
R_α(1/sec)	0	0	1.68×10^{-7}	1.00×10^{-6}	6.00×10^{-5}
β	0.001	0	0	0	0

Temperature-independent: $\nu = 0.365$, $n = 3.3$, $B_1 = 0.05$, $p = 1.8$, $q = 1.35$

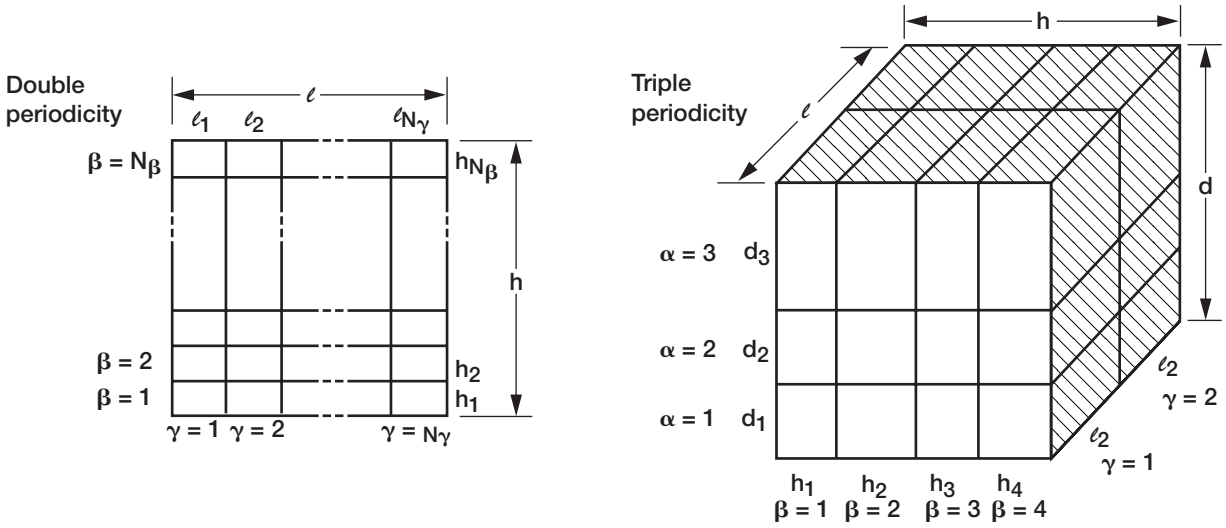

Figure 1.—Generalized Method of Cells, subcell dimension nomenclature for both (a) double and (b) triple periodicity conditions (reference 8).

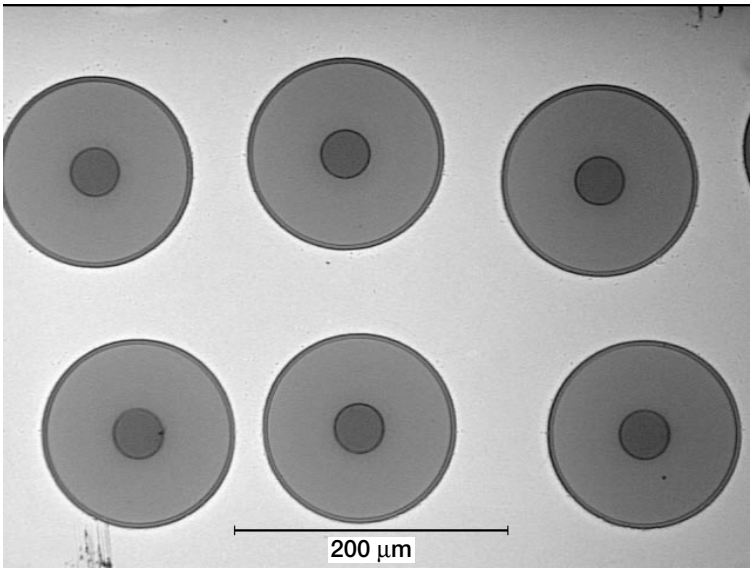

Figure 2.—Micrograph of SCS-6/TIMETAL 21S composite specimen.

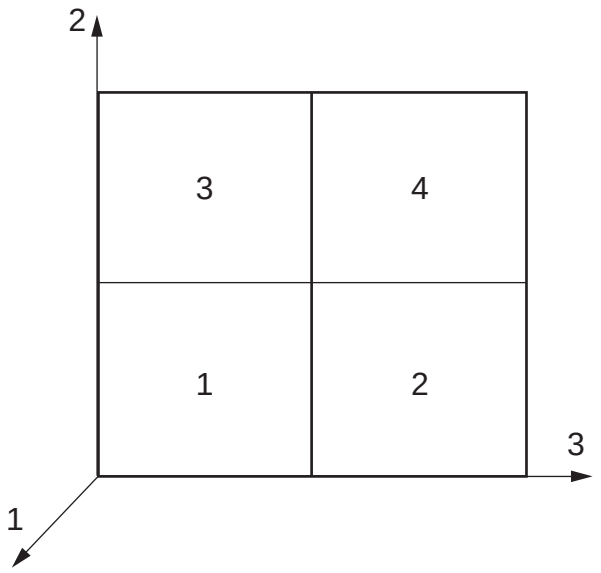

Figure 3.—Two-dimensional GMC model utilized to simulate longitudinal and transverse tensile loading (reference 8). For longitudinal loading, the loading direction was along the 1 direction axis. For transverse loading, the loading was along the 3 direction axis.

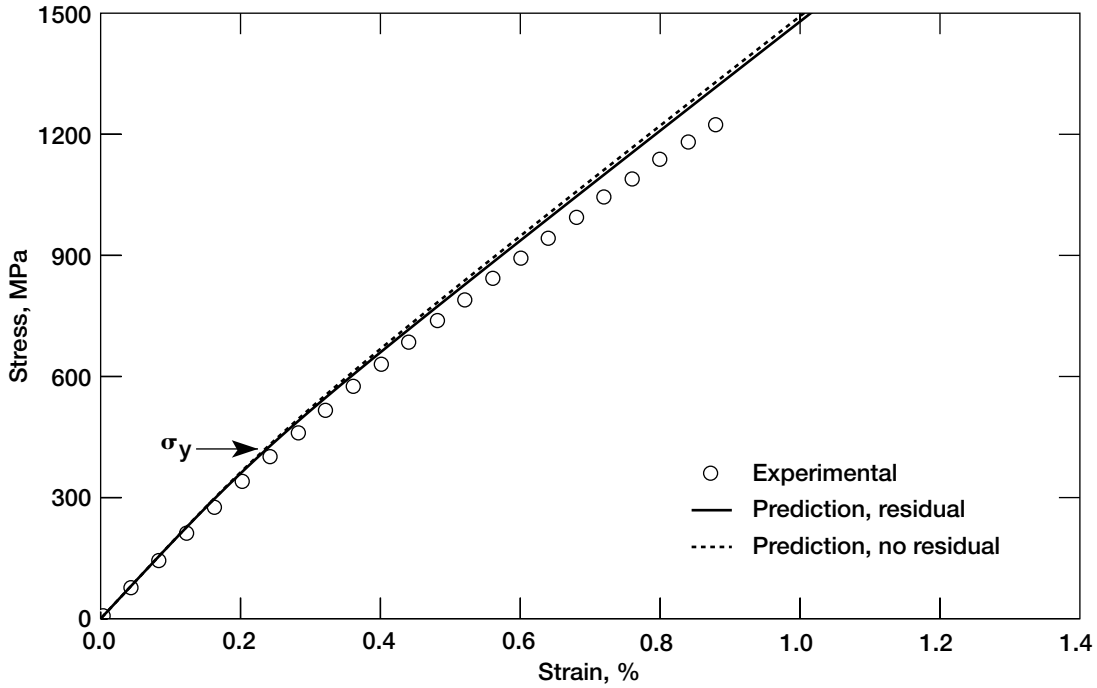

Figure 4.—Predicted longitudinal tensile stress-strain response of SCS-6/TIMETAL 21S at 650 °C with comparison to experiment (reference 27).

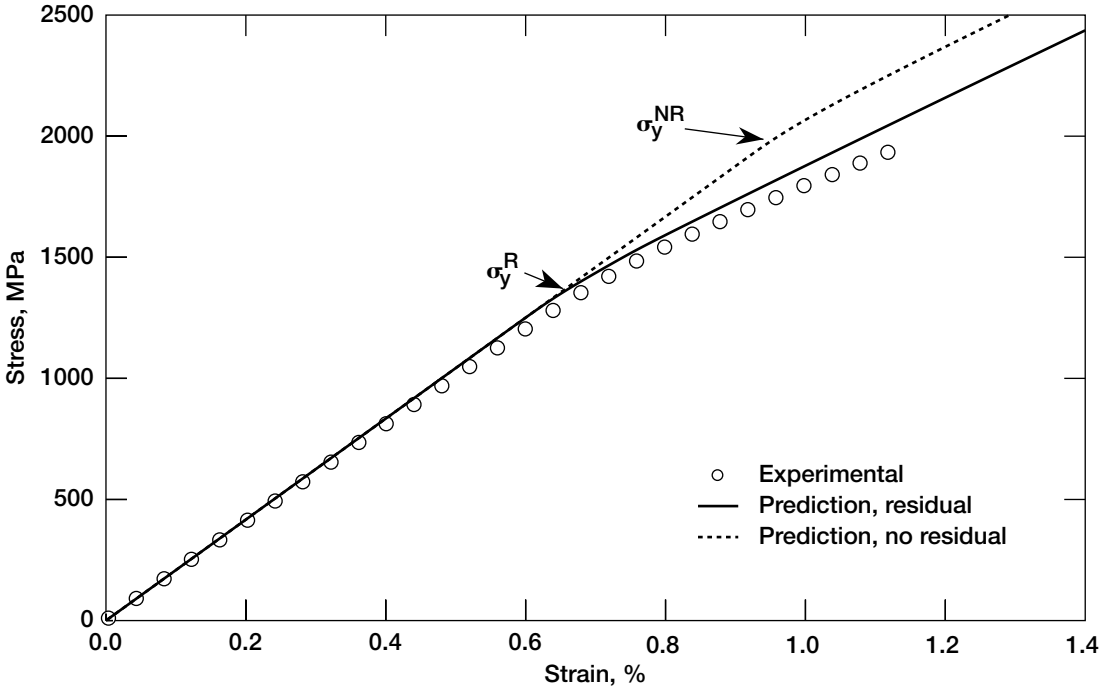

Figure 5.—Predicted longitudinal tensile stress-strain response of SCS-6/TIMETAL 21S at 23 °C with comparison to experiment (reference 27).

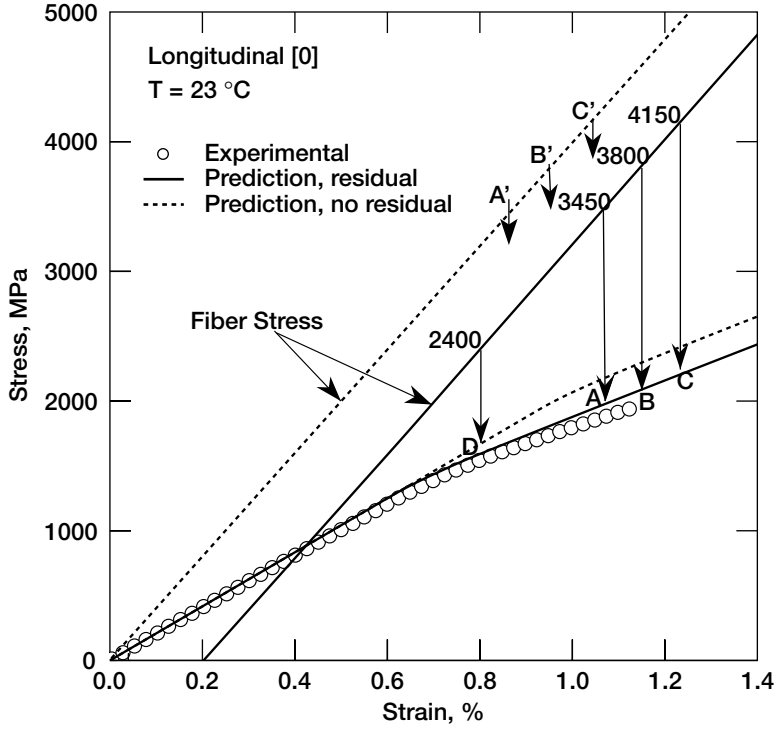

Figure 6.—Predicted longitudinal tensile stress-strain response of SCS-6/TIMETAL 21S at 23 °C with fiber response and fiber failure stresses included.

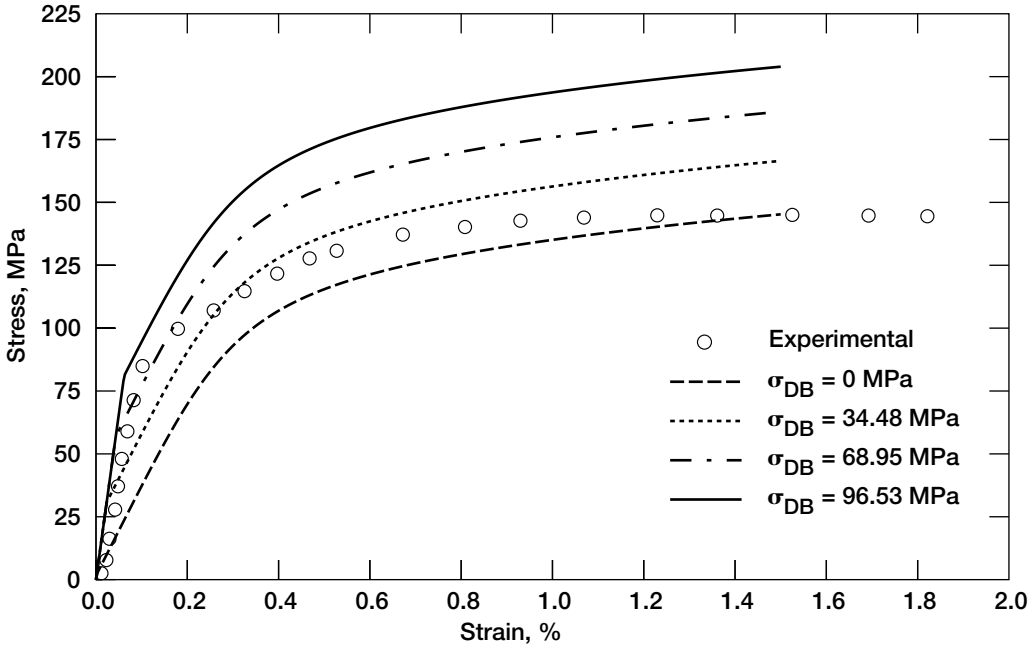

Figure 7.—Effect of debond stress on the predicted transverse tensile response of SCS-6/TIMETAL 21S at 650 °C with comparison to experiment (reference 26).

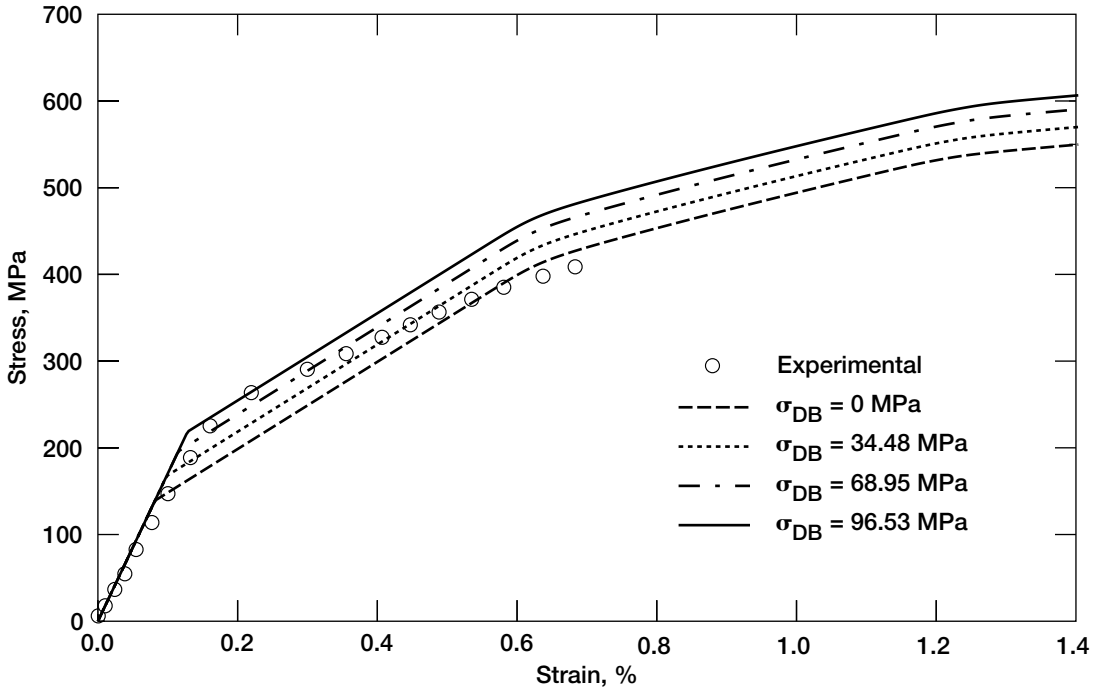

Figure 8.—Effect of debond stress on the predicted transverse tensile response of SCS-6/TIMETAL 21S at 23 °C with comparison to experiment (reference 26).

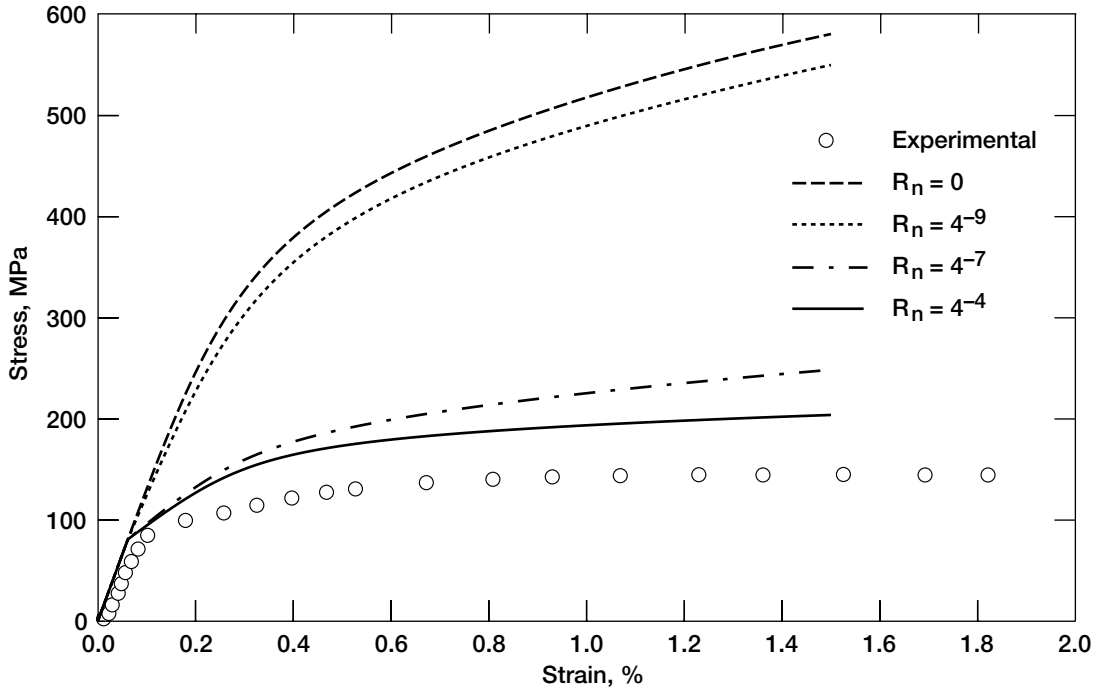

Figure 9.—Effect of interfacial compliance on the predicted transverse tensile response of SCS-6/TIMETAL 21S at 650 °C with comparison to experiment (reference 26).

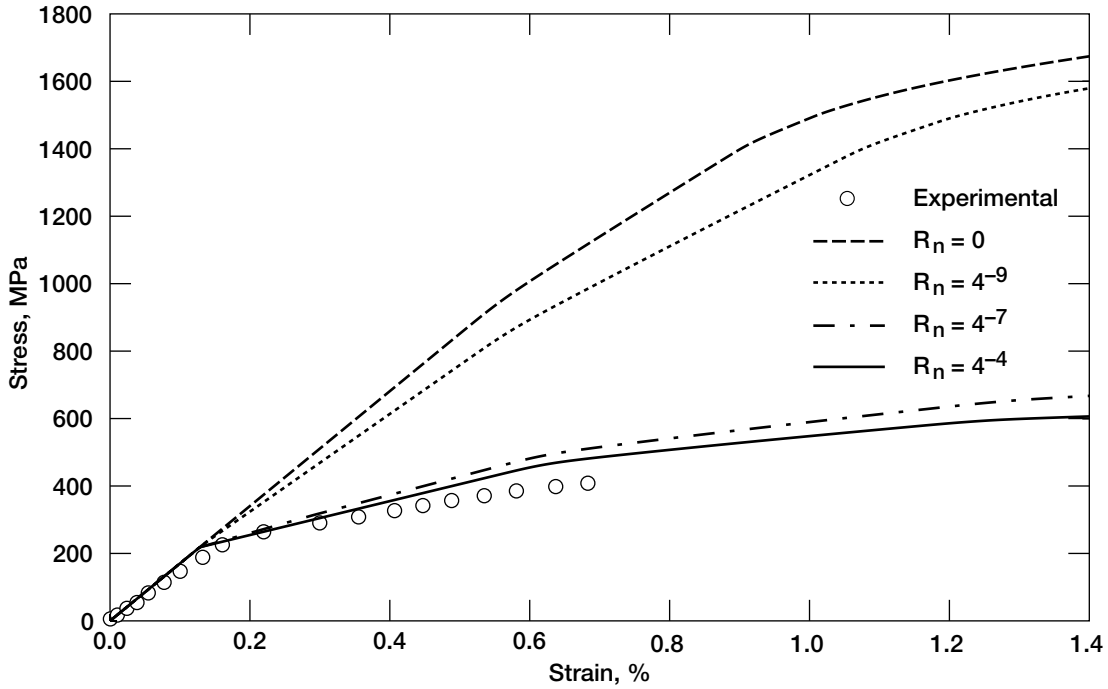

Figure 10.—Effect of interfacial compliance on the predicted transverse tensile response of SCS-6/TIMETAL 21S at 23 °C with comparison to experiment (reference 26).

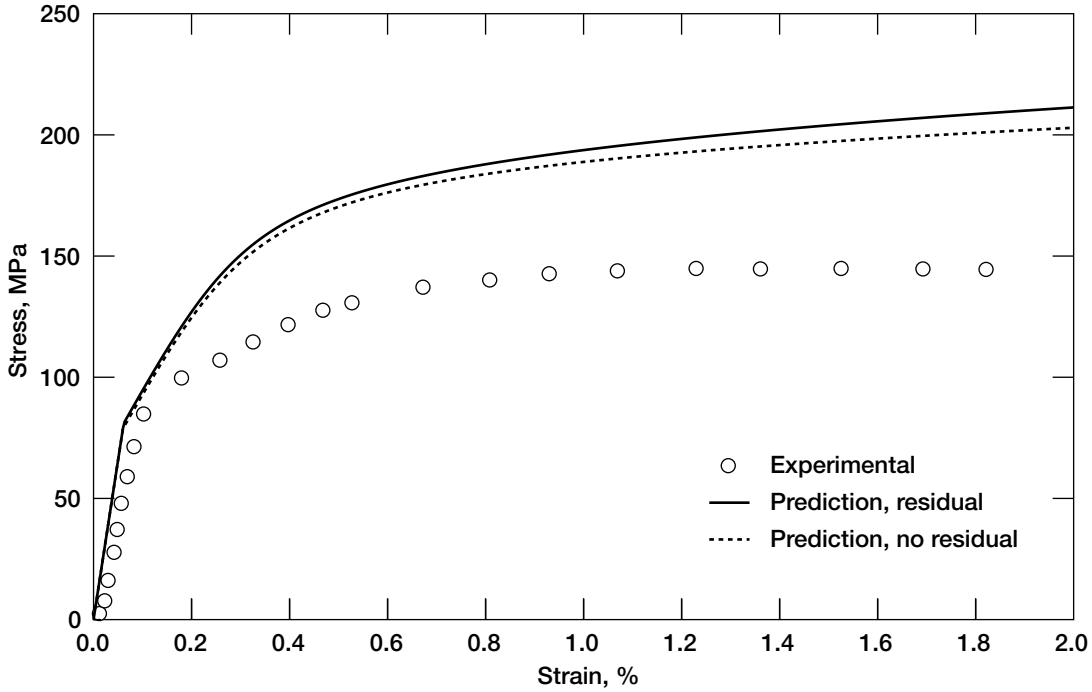

Figure 11.—Effect of residual stresses on the predicted transverse tensile response of SCS-6/TIMETAL 21S at 650 °C with comparison to experiment (reference 26).

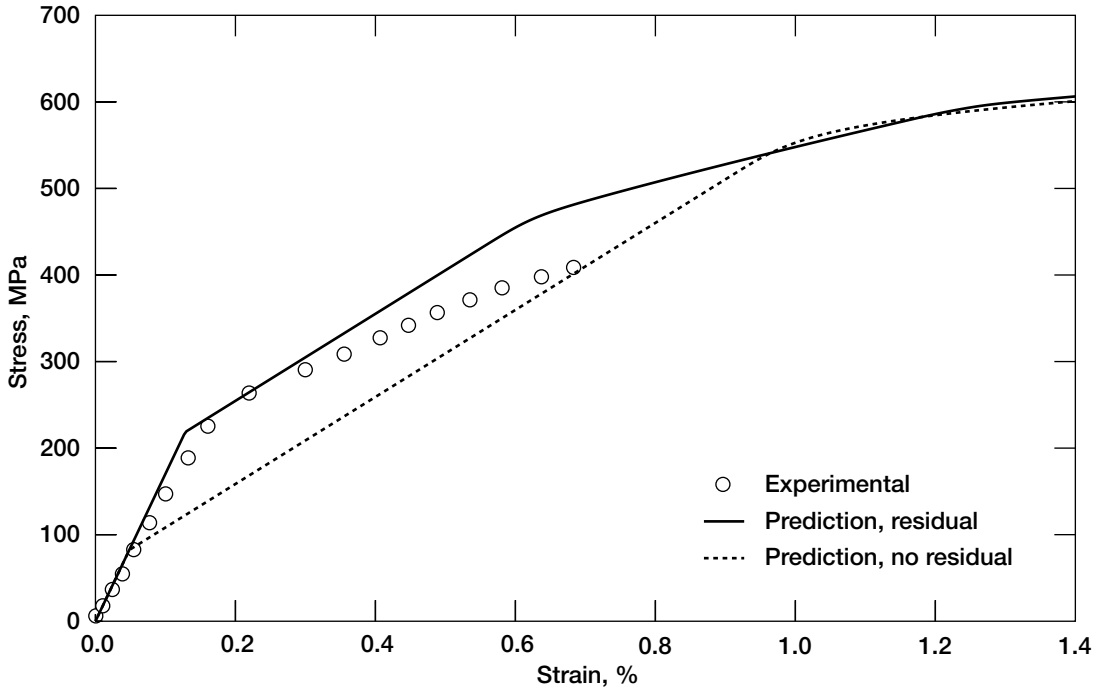

Figure 12.—Effect of residual stresses on the predicted transverse tensile response of SCS-6/TIMETAL 21S at 23 °C with comparison to experiment (reference 26).

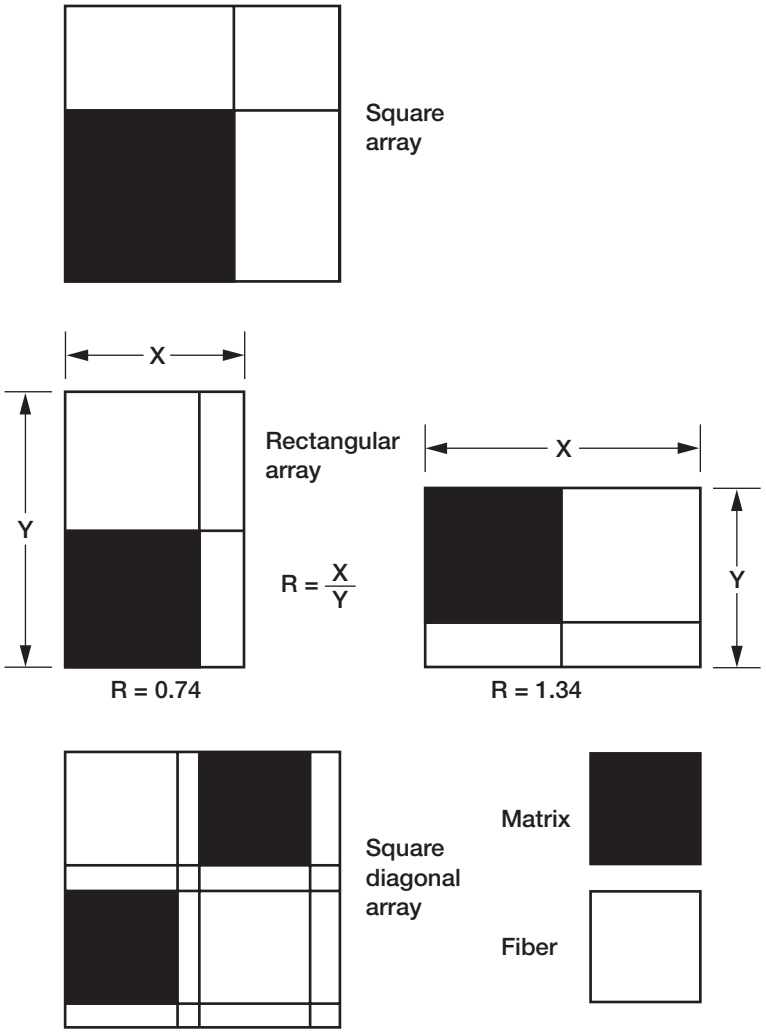

Figure 13.—Schematics of representative volume elements of the fiber packing arrays examined, including square, rectangular with R = 0.74 and R = 1.34, and square diagonal (reference 8). Transverse tensile loading is along 3 direction axis.

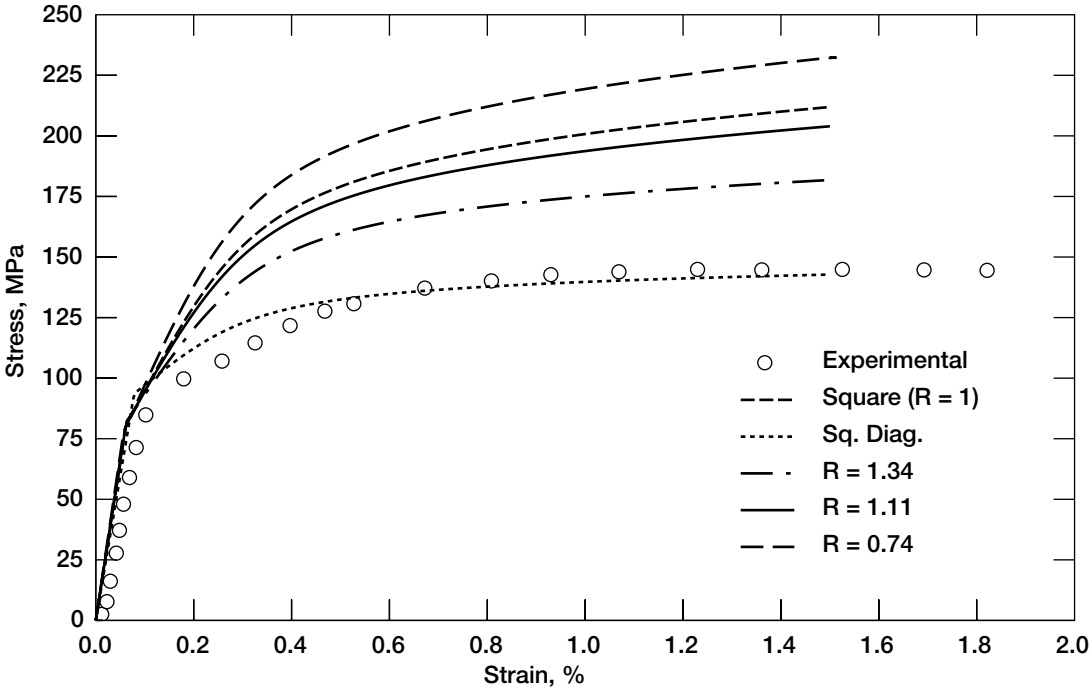

Figure 14.—Effect of fiber packing arrangement on the predicted transverse tensile response of SCS-6/TIMETAL 21S at 650 °C with comparison to experiment (reference 26).

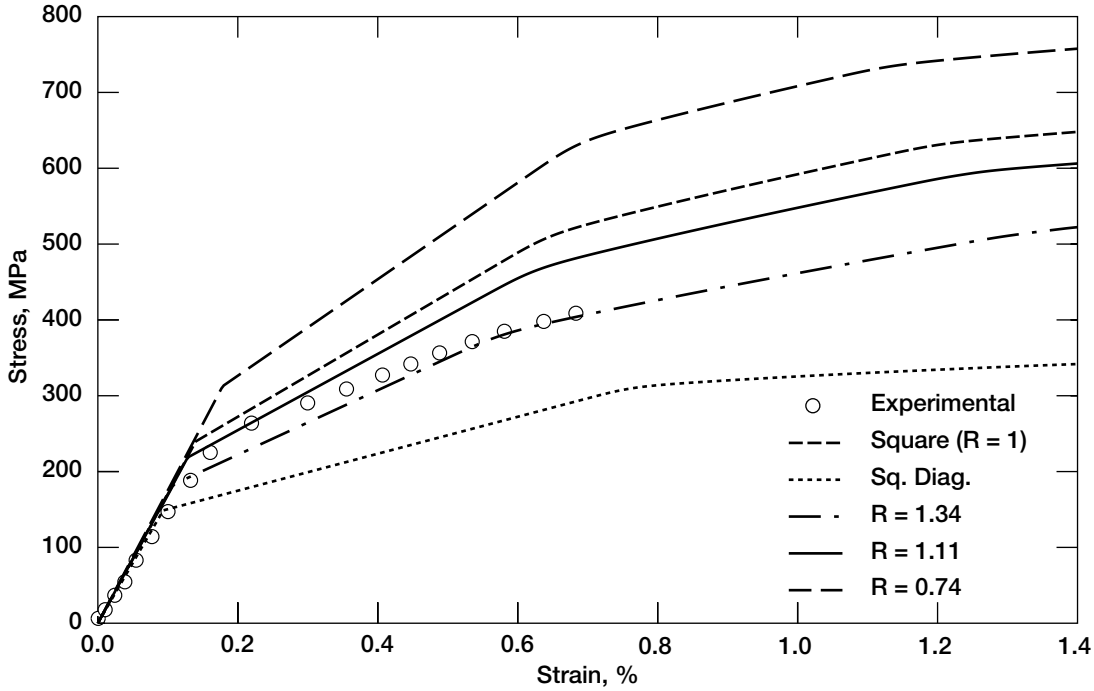

Figure 15.—Effect of fiber packing arrangement on the predicted transverse tensile response of SCS-6/TIMETAL 21S at 23 °C with comparison to experiment (reference 26).

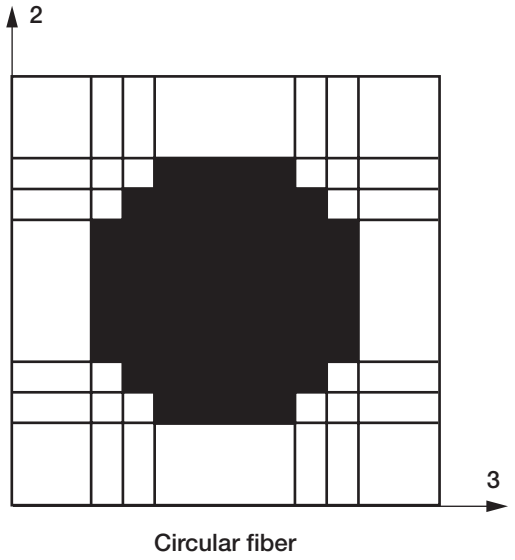

Figure 16.—Schematic of representative volume element with circular fiber shape (reference 8). Transverse tensile loading is along 3 direction axis.

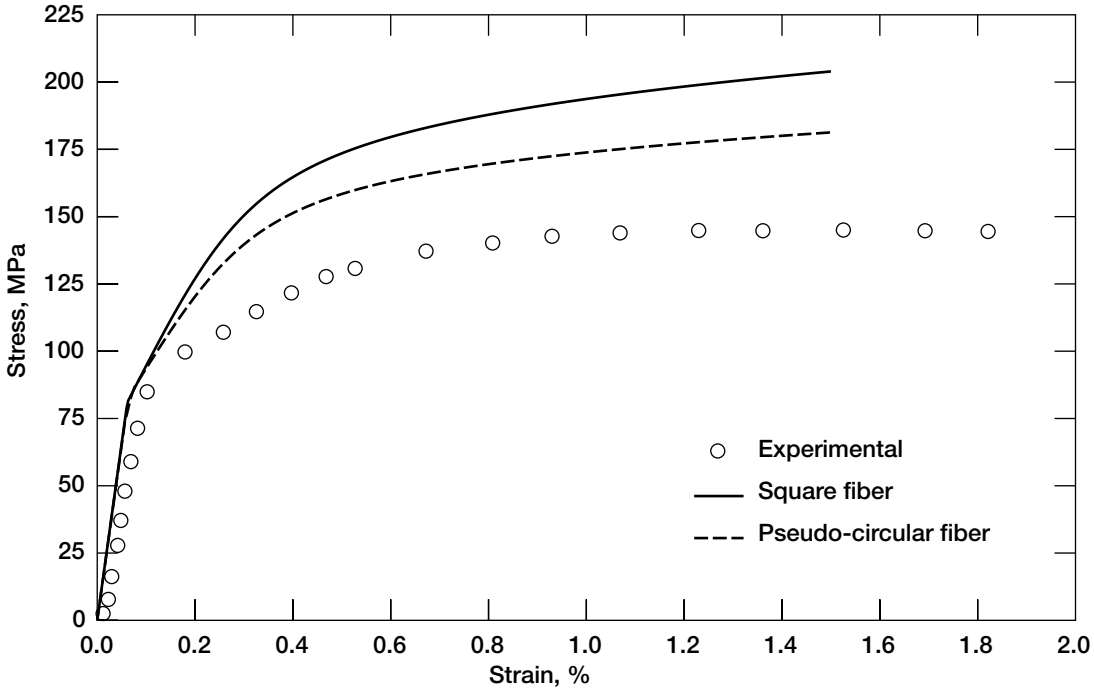

Figure 17.—Effect of fiber shape on the predicted transverse tensile response of SCS-6/TIMETAL 21S at 650 °C with comparison to experiment (reference 26).

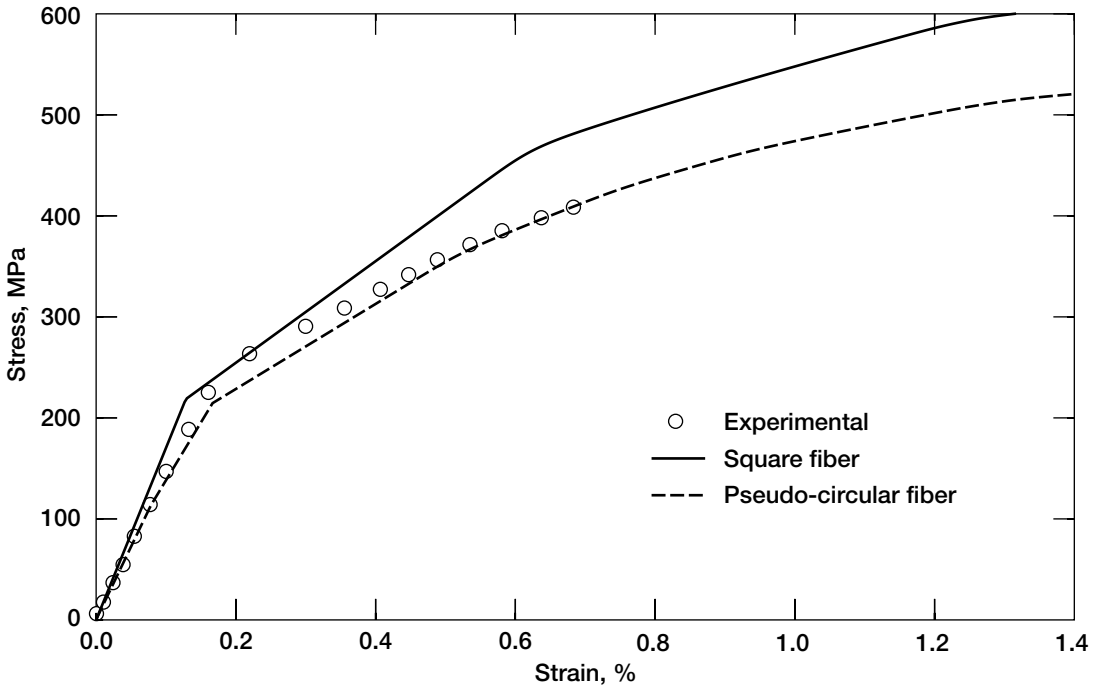

Figure 18.—Effect of fiber shape on the predicted transverse tensile response of SCS-6/TIMETAL 21S at 23 °C with comparison to experiment (reference 26).

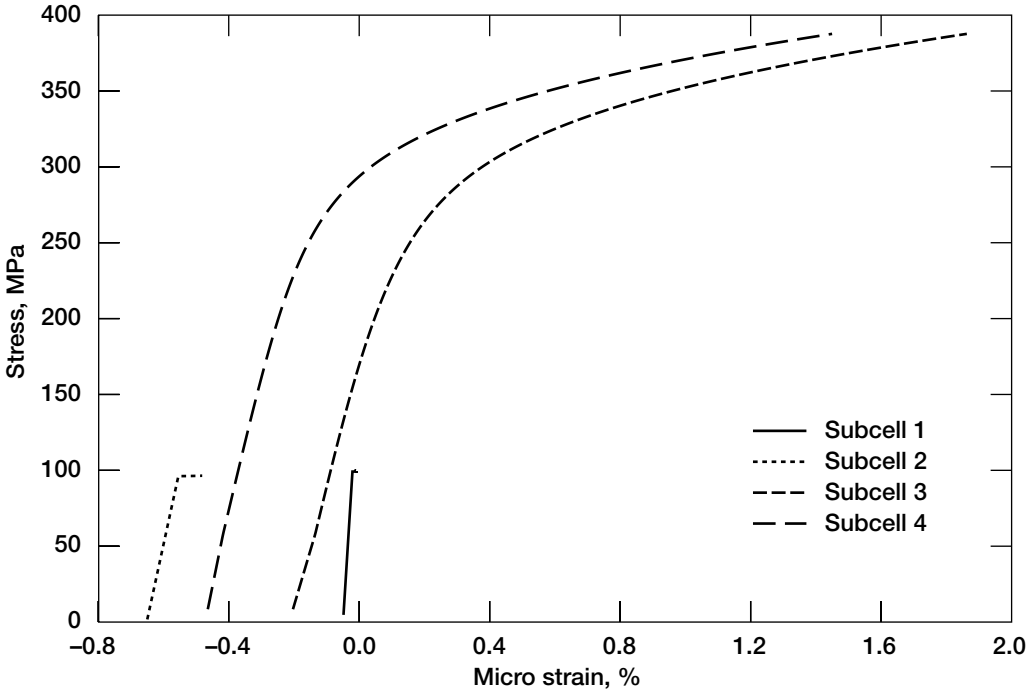

Figure 19.—Predicted transverse tensile stress vs. micro strain response of individual subcells of simulated SCS-6/TIMETAL 21S composite at 650 °C.

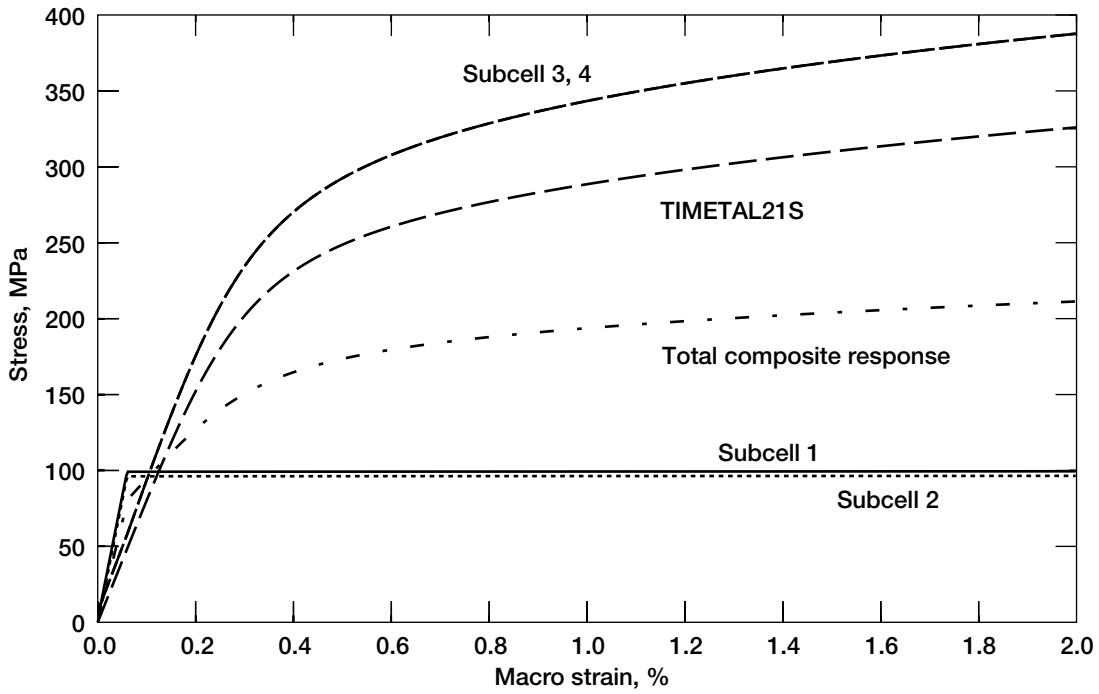

Figure 20.—Predicted transverse tensile stress vs. macroscopic strain response of individual subcells of simulated SCS-6/TIMETAL 21S composite at 650 °C. Predicted macroscopic response of composite and predicted response of bulk TIMETAL 21S included for comparison.

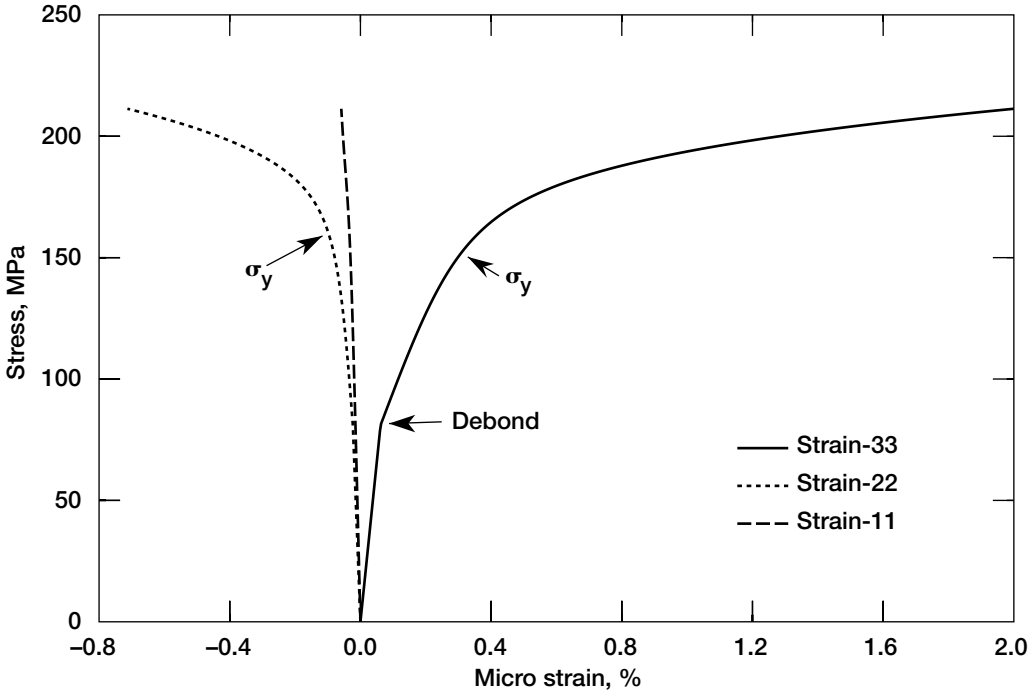

Figure 21.—Predicted transverse tensile stress/strain response of simulated SCS-6/TIMETAL 21S composite at 23 °C with off-axis strains included.

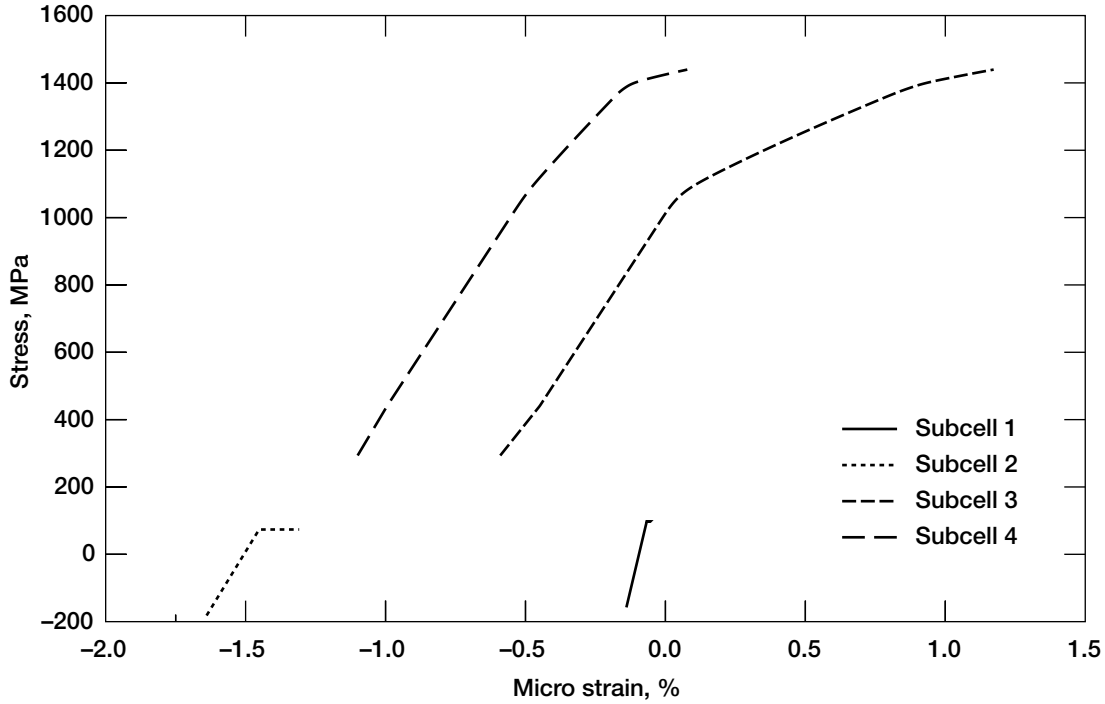

Figure 22.—Predicted transverse tensile stress vs. micro strain response of individual subcells of simulated SCS-6/TIMETAL 21S composite at 23 °C.

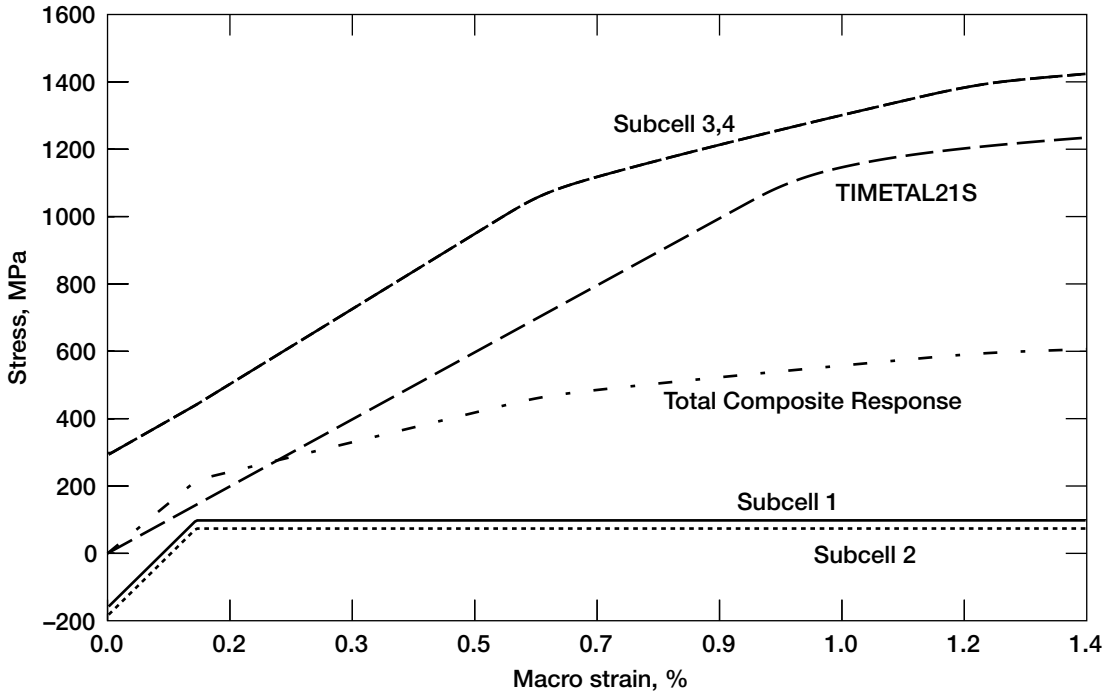

Figure 23.—Predicted transverse tensile stress vs. macroscopic strain response of individual subcells of simulated SCS-6/TIMETAL 21S composite at 650 °C. Predicted macroscopic response of composite and predicted response of bulk TIMETAL 21S included for comparison.

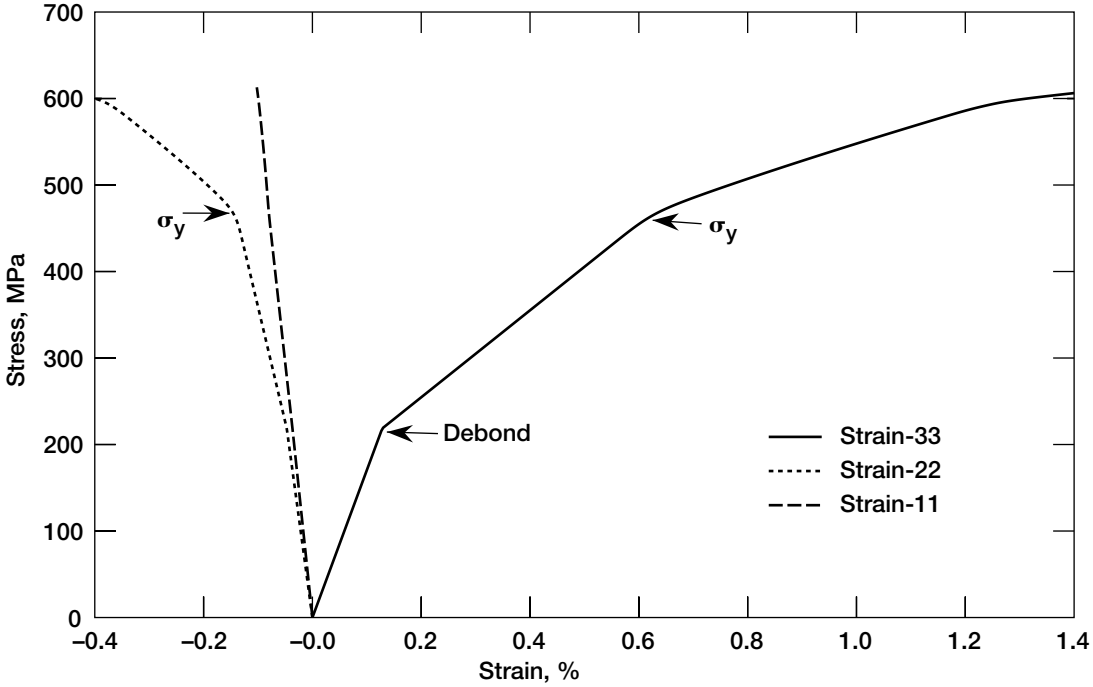

Figure 24.—Predicted transverse tensile stress/strain response of simulated SCS-6/TIMETAL 21S composite at 23 °C with off-axis strains included.

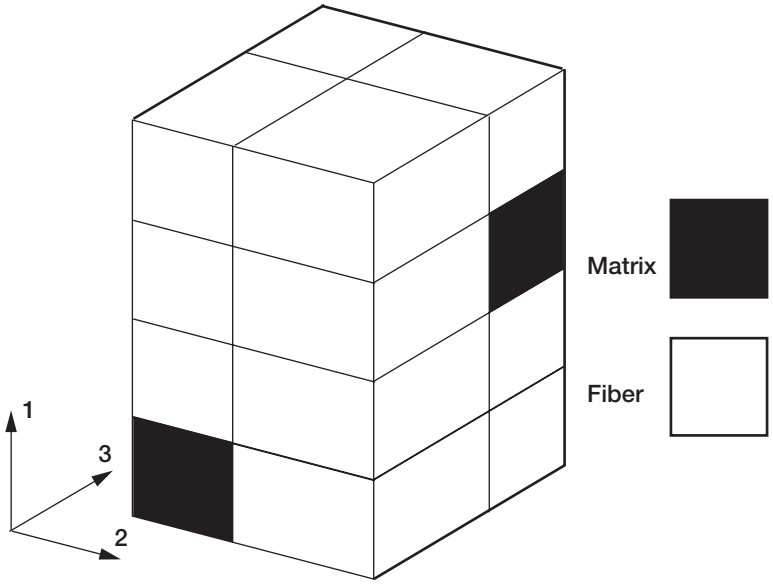

Figure 25.—Three-dimensional GMC model used to simulate tensile response of SCS-6/TIMETAL 21S [0/90] laminate (reference 8). The loading direction was along the 3 direction axis.

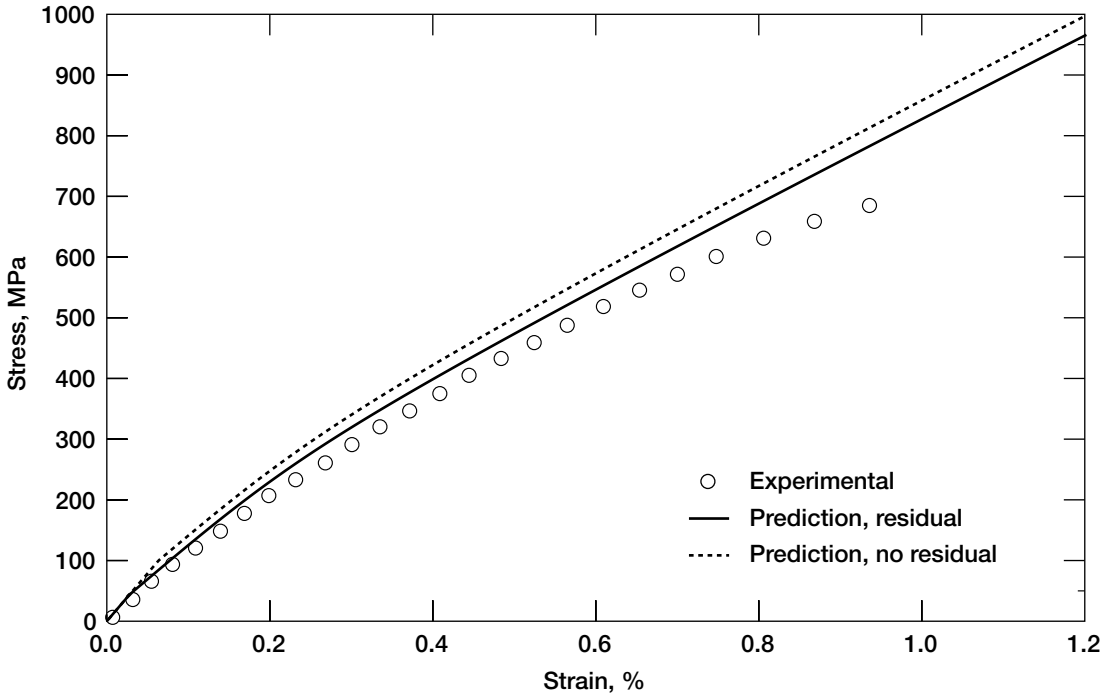

Figure 26.—Predicted tensile stress-strain response of SCS-6/TIMETAL 21S [0/90] laminate at 650 °C with comparison to experiment (reference 31).

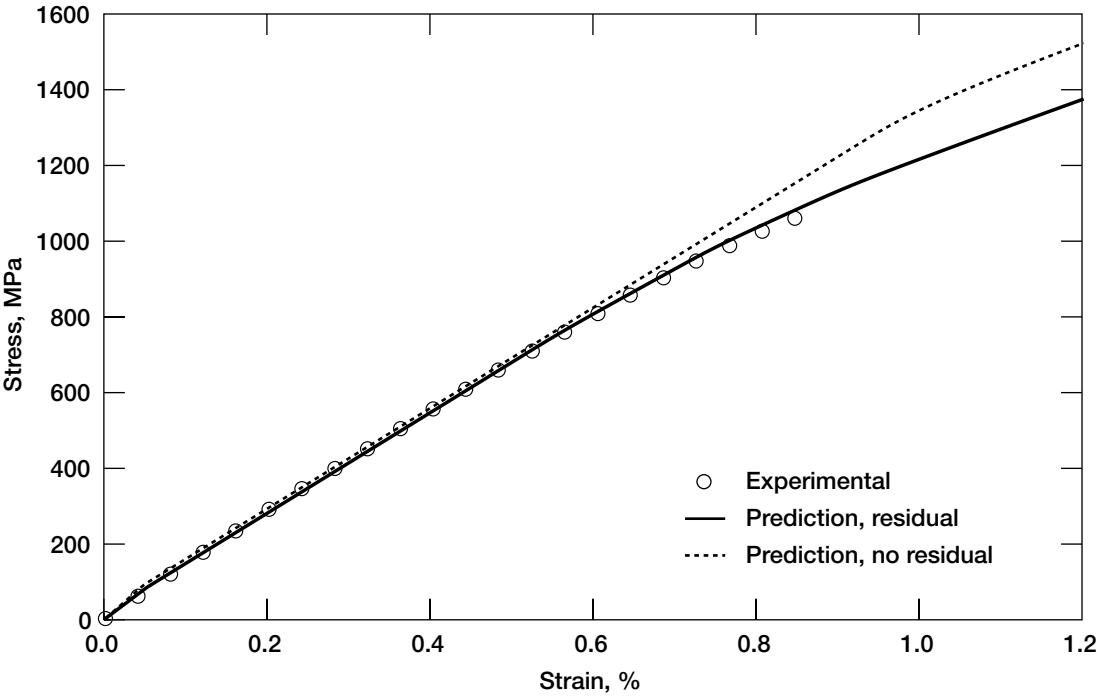

Figure 27.—Predicted tensile stress-strain response of SCS-6/TIMETAL 21S [0/90] laminate at 23 °C with comparison to experiment (reference 31).

REPORT DOCUMENTATION PAGE

Form Approved
OMB No. 0704-0188

1. AGENCY USE ONLY (*Leave blank*)	2. REPORT DATE	3. REPORT TYPE AND DATES COVERED
	March 2000	Technical Memorandum

4. TITLE AND SUBTITLE

A Study of Influencing Factors on the Tensile Response of a Titanium Matrix Composite With Weak Interfacial Bonding

5. FUNDING NUMBERS

WU–242–23–52–00

6. AUTHOR(S)

Robert K. Goldberg and Steven M. Arnold

7. PERFORMING ORGANIZATION NAME(S) AND ADDRESS(ES)

National Aeronautics and Space Administration
John H. Glenn Research Center at Lewis Field
Cleveland, Ohio 44135–3191

8. PERFORMING ORGANIZATION REPORT NUMBER

E–12089

9. SPONSORING/MONITORING AGENCY NAME(S) AND ADDRESS(ES)

National Aeronautics and Space Administration
Washington, DC 20546–0001

10. SPONSORING/MONITORING AGENCY REPORT NUMBER

NASA TM—2000-209798

11. SUPPLEMENTARY NOTES

Responsible person, Robert K. Goldberg, organization code 5920, (216) 433–3330.

12a. DISTRIBUTION/AVAILABILITY STATEMENT

Unclassified - Unlimited
Subject Category: 24 Distribution: Nonstandard

This publication is available from the NASA Center for AeroSpace Information, (301) 621–0390.

12b. DISTRIBUTION CODE

13. ABSTRACT ***(Maximum 200 words)***

The generalized method of cells micromechanics model is utilized to analyze the tensile stress-strain response of a representative titanium matrix composite with weak interfacial bonding. The fiber/matrix interface is modeled through application of a displacement discontinuity between the fiber and matrix once a critical debonding stress has been exceeded. Unidirectional composites with loading parallel and perpendicular to the fibers are examined, as well as a cross-ply laminate. For each of the laminates studied, analytically obtained results are compared to experimental data. The application of residual stresses through a cool-down process was found to have a significant effect on the tensile response. For the unidirectional laminate with loading applied perpendicular to the fibers, fiber packing and fiber shape were shown to have a significant effect on the predicted tensile response. Furthermore, the interface was characterized through the use of semi-empirical parameters including an interfacial compliance and a "debond stress;" defined as the stress level across the interface which activates fiber/matrix debonding. The results in this paper demonstrate that if architectural factors are correctly accounted for and the interface is appropriately characterized, the macro-level composite behavior can be correctly predicted without modifying any of the fiber or matrix constituent properties.

14. SUBJECT TERMS	15. NUMBER OF PAGES
Composites; Micromechanics; Viscoplasticity	33
	16. PRICE CODE: A03

17. SECURITY CLASSIFICATION OF REPORT	18. SECURITY CLASSIFICATION OF THIS PAGE	19. SECURITY CLASSIFICATION OF ABSTRACT	20. LIMITATION OF ABSTRACT
Unclassified	Unclassified	Unclassified	